UNIVERSITY OF EMBU

GRACE WAKARIMA NDIRITU

MSc

2019

CRAMÉR-RAO BOUND OF DIRECTION-FINDING USING UNIFORM HEXAGONAL ARRAY

NDIRITU WAKARIMA GRACE (BSC)

A RESEARCH PROJECT SUBMITTED IN PARTIAL FULFILLMENT FOR THE DEGREE OF MASTER OF SCIENCE IN APPLIED MATHEMATICS IN THE UNIVERSITY OF EMBU

SEPTEMBER, 2019

DECLARATION

This research project is my original work and has not been presented for a degree in any other University.

Signature…… Date……

Grace Wakarima Ndiritu
Department of Mathematics, Computing and Information technology
B527/1141/2017

This project has been submitted for examination with our approval as the University Supervisors

Signature…… Date…….

Dr. Dominic Makaa Kitavi.
Department of Mathematics, Computing and Information technology
University of Embu.

Signature…… Date…….

Dr. Cyrus Gitonga Ngari.
Department of Mathematics, Computing and Information technology
University of Embu

DEDICATION

To my beloved mother Mrs. Wanjiru Ndiritu and my siblings for their unconditional support and endless love that they accorded me during the enduring moment.

ACKNOWLEDGEMENT

I would like to thank all the people that supported me during my master's study and contributed to this project in various ways.

First, I would like to acknowledge my sponsors, the University of Embu for funding my studies. My deepest thanks go to my supervisors Dr. Dominic Kitavi and Dr. Cyrus Ngari, for their support, care, encouragements, and for giving me the opportunity to pursue my master's studies under their supervision. Special thanks to the department of MCIT for all the valuable support. In addition, I would like to thank my fellow graduate students Veronicah Nyokabi and Davis Kinyili for their valuable help and team spirit.

My deep and sincere gratitude to my mother for always encouraging me to work hard, study hard, and aim high, my brother, my sisters, and my late father for their continuous support and unconditional love.

Most of all, I would like to thank Almighty God, for the blessings and sound belief in Him, health, and sanity and for putting me in a path that allowed me to meet people that have been kind to me and allowing me the opportunity to reciprocate.

TABLE OF CONTENTS

LIST OF FIGURES

LIST OF APPENDICES

LIST OF MATHEMATICAL NOTATIONS

NOTATION	DESCRIPTION
$\boldsymbol{\Lambda}$	Wavelength
$\boldsymbol{\theta, \varphi, \beta}$	Unknown deterministic parameters
$\boldsymbol{\Omega}$	Wave angular frequency
$\boldsymbol{\Sigma}$	Variance
$\otimes$	Kronecker product
S	Incident signal
$\boldsymbol{\mu}$	Expected value
Γ	Covariance matrix
$*$	Off diagonal terms
$\boldsymbol{A_m}$	Excitation amplitude
A	Array manifold vector
c	Speed of light
d	Signal amplitude
D	Normalization constant
E [·]	Expectation of the identity under the square brackets
F	Frequency
$\boldsymbol{f(\sigma_c)}$	Phase induced by characteristic of lens
L	Number of array elements
K	Time index
N	Noise
$\boldsymbol{T}$	Transpose
$\boldsymbol{Q}$	Wave number
Re{.}	Real value of identity inside the curly brackets
H	Conjugate transpose
$I_{(L_x+L_y-z)M}$	Identity matrix of size $L_x + L_y - z)M$
$\boldsymbol{L_x}$	Number of sensors uniformly spaced
(α, **β**)	Unknown parameters
$\boldsymbol{J_m}$	m^{th} sensors stochastic complex gain

n(m)	Additive white Gaussian noise
φ	Phase
σ	Amplitude
$\boldsymbol{d}_l$	Sensor location
$I_{(LM)}$	$LM \times LM$ identity matrix
$\boldsymbol{\xi}$	Scalar parameters
$\odot$	Hadamard product
$\boldsymbol{\omega}$	Angular frequency
Tr{.}	Trace of entity inside the curly brackets
$\check{\boldsymbol{z}}$	Observations
$\check{\mu}$	Mean

LIST OF ABBREVIATIONS

ABREVIATIONS	DESCRPTION
1D	One Dimension
2D	Two Dimension
3D	Three Dimension
CCRB	Conditional Cramér-Rao bound
CRB	Cramér-Rao bound
CRLB	Cramér-Rao lower bound
DOA	Direction of arrival
DLSA	Double L-shaped array
DUCA	Double uniform circular array
ESM	Electronic surveillance measure
ESPRIT	Estimation of Signal Parameters via Rotational Invariance Techniques
FIM	Fisher information matrix
JKIA	Jomo Kenyatta international airport
LSA	L-shaped array
ML	Maximum likelihood
MSE	Mean square error
MUSIC	Multiple Signal Classification
MVUE	Minimum variance unbiased estimator
NSCA	Nested sparse circular array
RMSE	Root mean square error
R-MUSIC	Root-Multiple Signal Classification
PDF	Probability density function
SLL	Side-lobe level
SNR	Signal-to-Noise Ratio
UCRB	Unconditional Cram´er-Rao bound
UCA	Uniform circular array
UHA	Uniform hexagonal array
ULA	Uniform linear array

URA	Uniform rectangular array

ABSTRACT

Direction-of-arrival (DOA) estimation is an important branch in the field of array signal processing. It can be applied in such fields as wireless communication, sonar, radar, biomedicine, and radio detection. This fact together with the development of the geometries used in the past years is the principal motivation of this research project. Although various studies have focused on the uniform hexagonal array for direction finding, there is scanty use of the uniform hexagonal array in conjunction with Cram´er-Rao bound for direction finding. In this research project, the direction-of-arrival estimation of Cram´er-Rao bound based on the uniform hexagonal array was studied. The proposed approach concentrated on deriving the array manifold vector for the uniform hexagonal array and Cram´er-Rao bound of the uniform hexagonal array. The Cram´er-Rao bound based on the uniform hexagonal array were compared with Cram´er-Rao bound based on the uniform circular array. The array manifold vector and Cram´er-Rao bound for the uniform hexagonal array were derived. The Cram´er-Rao bound based on the uniform hexagonal array was compared with Cram´er-Rao bound of uniform circular array. The conclusions are as follows, the Cram´er-Rao bound of uniform hexagonal array decreases with an increase in the number of sensors, whereas that of circular array reduces with increase in the number of sensors. The comparison between the uniform hexagonal array and uniform circular array shows that the Cram´er-Rao bound of the uniform hexagonal array was slightly higher as compared to the Cram´er-Rao bound of the uniform circular array. Thus, uniform circular array is a better approximator as compared to uniform hexagonal array. Graphical representation validated the analytical result.

CHAPTER ONE

INTRODUCTION

1.1 Background of the study

In signal processing, the direction of arrival (DOA) estimation denotes the direction from which a propagating wave arrives at a point, where a set of sensors are placed. The DOA estimation of the impinging signal is a significant technique in array processing. In the last few decades, DOA has received a considerable amount of interest in the field of military, wireless communication, sonar, radar, among others [1]. In radar, it's used to determine the location of an aircraft, taking an example of airport surveillance radar, it's used to ascertain the scope of an aircraft. In sonar, it is used to determine the location of the target such as submarine [2]. Military use direction beams to hide transmissions from the enemy [3]. Mechanically steered narrow-beam antennas were used to estimate the DOA of the impinging signal in earlier days. A wide range of mathematical algorithms has become available for DOA estimation due to the introduction of digital signal processor [4]. The main objective of estimating the DOA using different techniques is to obtain high resolution in direction finding estimates using the received data from a set of sensors [5].

Fisher information matrix (FIM) is a key concept in statistical signal processing. It basically characterizes the amount of information data provided about the unknown parameter. The higher the Fisher information matrix, the greater the accuracy with which the variable can be determined. Cram´er-Rao bounds (CRB) is equivalent to the inverse of the Fisher information matrix [6]. The most significant application of the FIM is in determining independent lower bound for the variance of unbiased estimator. Let $V(\boldsymbol{X})$ be any statistic and let $\delta(\theta)$ be its expectation, so that

$$var(V(\boldsymbol{X})) \geq \frac{\left(\frac{d\delta(\theta)}{d(\theta)}\right)^2}{I_n(\theta)}. \tag{1.10}$$

This is referred to as the Cram´er-Rao inequality. The value on the right-hand side of equation (1.10) is known as Cram´er-Rao bound. If $V(\boldsymbol{X})$ is an unbiased estimator for θ, then the numerator value becomes 1 [7].

Mean square error (MSE) measures the average mean squared deviation of the estimator from the true value, that is

$$\text{MSE}(\hat{\theta}) = E\left\{(\hat{\theta} - \theta)^2\right\}, \tag{1.11}$$

where $\hat{\theta}$ is an unbiased estimator and θ is the true value. Mean square error is equal to the variance (VAR) plus the bias of the estimator in the biased case, that is [4],

$$\begin{aligned}\text{MSE}(\hat{\theta}) &= E\left\{\left|\left(\hat{\theta} - E(\hat{\theta})\right) - \left(\theta - E(\hat{\theta})\right)\right|^2\right\} \\ &= VAR\{\hat{\theta}\} + \left|\theta - E(\hat{\theta})\right|^2. \end{aligned} \tag{1.12}$$

Mean square error is equal to the variance of the estimator as shown below

$$\text{MSE}(\hat{\theta}) = E\left\{\left|\hat{\theta} - E(\hat{\theta})\right|^2\right\} = VAR\{\hat{\theta}\}. \tag{1.13}$$

In order to understand the achievement of parameter estimation techniques, a set of bounds on their achievement is developed. These bounds are the Cram´er-Rao bounds. Thus, for any unbiased estimator

$$\text{MSE}(\hat{\theta}) = VAR\{\hat{\theta}\} \geq CRB. \tag{1.14}$$

It is assumed that the PDF satisfies the condition below

$$E\left[\frac{\delta \log \boldsymbol{p}(x;\theta)}{\delta\theta}\right] = 0. \tag{1.15}$$

The variance of any unbiased estimator satisfies

$$VAR\{\hat{\theta}\} \geq \frac{1}{-E\left[\frac{\delta^2 \log \boldsymbol{p}(x;\theta)}{\delta\theta^2}\right]}\ . \tag{1.16}$$

Cramér-Rao bound (CRB) expresses a lower bound on the variance of any unbiased estimator of a deterministic parameter [2]. CRB is used as a standard in the assessment of the accuracy of an estimator since its estimate can be evaluated for various practice settings and it is an important tool for practical design [8]. CRB can be used to forecast how a specific plan choice impacts the photometric and astrometric achievement of the designed instrument [6]. Cram´er-Rao bound is also used to describe the achievement of direction finding in antennas arrays. The most preferred achievement measure is the Cramér-Rao bound for any array geometry, regardless of the estimation technique used [9].

Determining a lower bound on the expectation of the squared deviation of a random variable from its mean of an unbiased estimator is very important. It helps to predict whether an estimator is a Minimum variance unbiased estimator (MVUE). This occurs if the assessor achieves the bound for the values of deterministic parameters [2]. Minimum variance unbiased estimator (MVUE) do not commonly prevail and when they do, various methods can be used to obtain them. These methods depend on the (CRB). The estimator is said to be unbiased if its mean generates a true value of the unknown parameter. An estimator being unbiased does not mean that it is the best estimator, it only contracts that on average it will obtain the real value of the parameter [2].

The direction of arrival estimation greatly enhances communication and network capacity. Direction finding problem has been an active research area for decades and many methods have been used to solve this problem [10]. They include Maximum likelihood [3], Multiple Signal Classification (MUSIC) and Estimation of Signal Parameters via Rotational Invariance Techniques (ESPRIT). MUSIC and ESPRIT are Eigen decomposition algorithms, that determines the DOA estimation by decomposing the covariance matrix to get eigenvectors and eigenvalues [11]. Maximum Likelihood method maximizes the log-likelihood function in order to determine the direction of arrival estimation [10].

Uniform hexagonal array is a two-dimensional array manifold [3], that is widely used in practice but has obtained less attention in the field of array signal processing [12]. It occurs when the sensors are placed on a single hexagon with uniform spacing. In the last few decades, many array geometries have been used for direction finding they include uniform linear array (ULA) which occurs when the sensors are equally spaced along a straight line [13]. ULA has perfect orientation and forms a small main-lobe in a certain direction [6]. ULA cannot find a 2D direction of a signal and also when the number and the angular distance of sensors are increased to enhance the accuracy of direction finding, the array length increases resulting in the change of the array structure [14].

The uniform circular array (UCA) occurs if the sensors are placed on a single circle with uniform spacing [8]. The uniform rectangular array (URA) is a two-dimensional vector

array that occurs when the sensors are uniformly spaced on a rectangle [15]. A major disadvantage of URA is that an extra major lobe of similar strength emerges on the opposite side [3]. Non-uniform linear array (NLA) have been used to determine the direction of arrival estimation [16]. An L-shaped array consists of a one-dimension array whose axes are different have been used for direction of arrival estimation in conjunction with CRB [9]. UCA is able to provide 360 degrees of coverage in the azimuth plane [17]. MUSIC based on uniform circular array is compared to Music based on uniform linear array in direction finding. UCA performs better than ULA since its array size is small and it is easier to increase sensor to enhance the accuracy of direction of arrival estimation [14].

The parameters of DOA are obtained from the array manifold vector with a precision that depends on the estimation technique and array geometry [8]. A sensor array is a group of sensors usually deployed in a certain geometry pattern, for collecting and processing signals. Each sensor converts an electromagnetic wave into a voltage [18]. The merit of using an array of sensors over a single sensor is to obtain better performance [16]. Most of the methods used to determine DOA considers the intersensory spacing between any two sensors to be half wavelength on ULA. Nevertheless, in wireless communication, there are some cases where such half wavelength spacing is not relevant [16]. Digital sensors arrays have several merits over traditional arrays including enlarged coverage, expanded system capacity, and resistance to two waves superpose to form a resultant wave. They also have the ability to ascertain an incoming signal of direction finding [19].

1.2 Statement of the problem

The accuracy of direction finding had been conducted for the 3D planar array, nested sparse circular array (NSCA), an L-shaped array using Cramér-Rao bound method. The direction of arrival estimation using uniform hexagonal array had been conducted employing improved swarm optimization method and the global hybrid optimization method. Uniform circular array is the traditionally known best approximator of direction of arrival estimation using multiple signal classification, bistatic multiple-input multiple-output radar, and Cramér-Rao lower bound method. More recently, circular arrays have been proposed for direction finding in particular for sensor arrays unlike linear arrays, circular array can scan

horizontally for $360^0$with no distortions in the array pattern of a circular array. The direction of arrival estimation using a uniform hexagonal array, employing the Cramér-Rao bound method had not been addressed. This study, therefore, aimed at deriving array manifold, Cramér-Rao bound and comparing the Cramér-Rao bound of the uniform hexagonal array and uniform circular array. The geometry was centered at the origin of the Cartesian plane lying on the x-y plane. M number of isotropic sensors with equal inter-sensor spacing were uniformly spaced.

1.3 Justification of the study

An accurate direction of arrival is a challenging and interesting area in array signal processing. The increase in the direction of arrival estimation applications in our life has increased the requirements for accurate direction-finding estimation. One way of achieving these requirements is by using the Cramér-Rao method. Therefore, correct DOA estimation becomes more important in Wireless communication, radio astronomy, sonar, radar, navigation, and the tracking. In view of the weakness of the linear array and rectangular array, it is necessary to consider some other geometries, such as circular and hexagonal arrays. The study will improve the accuracy of direction of arrival and enhance application in various field. Researchers can use this study to improve the accuracy of direction of arrival, by deriving the Cramér-Rao bound of other polygons and comparing them with Cramér-Rao bound of a uniform hexagonal array and uniform circular array. The geometry that will have the lowest Cramér-Rao bound, will be the most appropriate geometry for direction of arrival estimation.

1.4 General objective

To determine the accuracy of direction of arrival estimation using Cramér-Rao bound based on the uniform hexagonal array and compare the Cramér-Rao bound of the uniform hexagonal array with that of the uniform circular array.

1.4.1 Specific objectives

1. To derive the array manifold vector for the uniform hexagonal array.
2. To derive the Cramér-Rao bound for the uniform hexagonal array.

3. To compare Cramér-Rao bound of the uniform hexagonal array and uniform circular array.

1.5 Scope of work

The scope of this research work was limited to a set of isotropic sensors that were uniformly distributed on the edge length and vertices of the uniform hexagonal array. The central point of the array was at the origin of a Cartesian coordinate system, which was the reference point. A complex-valued sinusoidal signal from a far-field source impinged on a set of the array of sensors at an azimuth angle of ϕ, which was measured counterclockwise from the positive x-axis, and a polar angle of θ measured clockwise from the positive z-axis. The signal was corrupted by a complex-valued Gaussian noise, with real-valued component statistically independent from the imaginary-valued component, with a known variance $\sigma^2$and a mean of 0. Azimuth angle and polar angle were modeled as deterministic but prior unknown. Observed data vector followed a normal/Gaussian distribution. Cramér-Rao bound of azimuth and the polar angle was obtained from the inverse of the Fisher information matrix.

.

CHAPTER TWO

LITERATURE REVIEW

In this chapter, the literature review of the array manifold for various geometries, Cramér-Rao bound and comparison of the achievement of different geometries was analyzed.

2.1 Array manifold vector

This section introduces the definition of the array manifold vector and its importance in the estimation of direction of arrival estimation. A tetrahedral array whose sensor fail randomly, tetrahedral array in conjunction with hybrid Cramér-Rao bound and uniform linear array manifold vector are provided in this section.

Array manifold vector refers to a set of data received on an array of sensors from an incoming signal. It varies depending on the pattern of the sensor under consideration [18]. The array manifold vector is one of the most important parameters of an array system. The characteristic of an array system can be assimilated in the array manifold, which denotes the responses of an array system. An array manifold is a geometric object, entrenched in a multidimensional complex space [20]. A regular tetrahedral array whose essential sensors fail unsystematic has been used for DOA estimation. A sensor can fail, to make up for such a scenario in DOA estimation, an estimated lower bound is defined. A simple statistical data model is assumed for the arriving signal and the corrupting noises in order to focus on the stochastic effects of sensor failure. A signal from a far-field source impinges on the tetrahedral array at an azimuth angle θ and polar angle ϕ. It is assumed that an m^{th} sensor is located on the (x_m, y_m, z_m). The whole tetrahedral array is described by 4×1 array manifold vector, whose m^{th} element is given by the equation

$$[\boldsymbol{a}(\boldsymbol{\theta}, \boldsymbol{\phi})]_m = e^{\frac{i2\pi}{\lambda}[x_m \sin(\theta)\cos(\boldsymbol{\phi}) + \boldsymbol{y_m} \sin(\theta)\sin(\boldsymbol{\phi}) + z_m \cos(\theta)]} . \quad (2.11)$$

To evaluate the azimuth-polar DOA estimation accuracy, the failure rate should approach zero while estimated lower bound should approach the CRLB [21].

A tetrahedral array of identical sensors is used for DOA estimation using the hybrid Cramér-Rao (HCRB). Each sensor is considered to be suffering a certain random complex gain. The first case to be considered is when each sensor suffers an uncertainty in its complex gain. The tetrahedral array was made up of four sensors with equal inter-sensor spacing. M number of identical sensors that are separately located in space is considered. The three-dimensional location of the m^{th} sensor is denoted as x_m, y_m, z_m. An incident signal of wavelength λ, arriving on an array of sensor from an elevation angle θ and an elevation angle ϕ, specified with respect to the positive x-axis. The array manifold vector is characterized by an $M \times 1$ array response whose m^{th} entry equals

$$[\boldsymbol{a}]_m = g_m e^{\frac{i2\pi}{\lambda}[x_m \sin(\theta)\cos(\boldsymbol{\phi}) + \boldsymbol{y_m} \sin(\theta)\sin(\boldsymbol{\phi}) + z_m \cos(\theta)]} \quad (2.12)$$

where g_m denotes sensor's stochastic complex gain. The sensor stochastic complex gain affects the (HCRB) through multiplicative factor [22]. Successful performance analysis method is used to evaluate array manifold of Uniform linear array, to enhance DOA estimation performance. The expression of the array manifold vector is expressed as follows

$$\mathbf{a}(\boldsymbol{\phi_i}) = \left[\mathbf{p_1}(\phi_i)e^{-i\boldsymbol{\omega\tau_1}}, \mathbf{p_2}(\phi_i)e^{-i\omega\tau_2}, \mathbf{p_3}(\phi_i)e^{-i\omega\tau_3} \ldots, \mathbf{p_n}(\phi_i)e^{-i\omega\tau_n}\right]^{\boldsymbol{T}}. \quad \textbf{(}2.13\textbf{)}$$

The results above shows that DOA estimation achievement can be enhanced by increasing the aperture of the array antenna [11].

Array signal processing (ASP) is a new algorithm in Digital Signal Processing with many applications. ASP is the quickest growing area of electrical engineering. It is an active area and involves analyzing the data received on the array of sensors [14]. In order for the array of sensors to be able to give the necessary functionality and gain of the transmission, they need to be able to discern the direction of arrival (DOA) of the needed impinging signal [23]. It is a wide area of research that extends from the simplest 1D to the complex form of MD. DOA is a parameter estimated from the collected information. Determining the position of the object or DOA of a signal is one of the expounded estimation tasks. Direction-of-arrival (DOA) estimation refers to an angle at which a signal impinges on the array of sensors. To approximate the DOA of the signal, we need to estimate the azimuth and polar angles in regard to the incoming signals [10].

In the last few decades, accurate determination of DOA from a signal source has received a considerable amount of interest in various fields such as wireless communication, radar, sonar and military [10]. In the last decade, DOA estimation has been focusing on approximating the direction of electromagnetic waves arriving on the array of sensors [24]. An accurate DOA estimation of the signal from a far-field source to a receiving sensors array can increase the wireless communication systems capacity [25]. The array of sensor can either be passive or active. In a passive system, the sensor array has the task of listening to the environment. In this case, the energy source is the target itself. In an active system, on the other hand, a transmitter emits energy to the environment and the sensor array listens to the environment for the response of the target [26].

2.2 Cramér-Rao bound method

This section introduces the definition of the Cramér-Rao bound (CRB), the uses of the CRB, how it has been used for direction finding in various geometries and finally, how it has been used in conjunction with other techniques for accuracy of direction of arrival estimation.

CRB is a lower bound on the variance of any unbiased estimator. The derivation of the CRB depends on the assumed model for the received signal and the parameters to be estimated. Determining the CRB helps to provide a form for minimum variance unbiased estimator, demonstrates the importance of the proposed estimators and also helps on the judgment of the proposed estimators [2]. The higher the SNR the lower the CRB. It is used as a performance measure which under planar and coplanar array is obtained from the inverse of the Fisher information matrix. When the array is planar the CRB is further simplified, since a fixed source polar angle becomes a cosine function of the azimuth source [27]. The use of the polar coordinate system to define sensor positions can give a more compressed expression of the CRB, on the other hand, a cartesian coordinate system is useful for specifying how CRB is affected by a particular array geometry [28].

CRB is an important benchmark used to assess the achievement of various unbiased estimators. It is applied in communication and signal processing fields. The estimation accuracy of the near-field array manifold through the derivation of the CRBs have been analyzed. The CRB of distance increases linearly with an increase in distance wherever the sources are near the sensor. The CRB is dependent on the distance between the sources and sensors in the Gaussian source scenario. However, in polynomial-phase source scenario, the CRB of the angle of arrival do not depend on the distance [29]. Stochastic CRB on DOA estimation accuracy has been derived for non-circular Gaussian sources. Stochastic CRB of a closed-form expression for DOA parameters is derived directly from Slepian-bangs formula [30].

The achievement of high-resolution DOA estimation method is evaluated using stochastic and deterministic CRBs. Two approaches are considered in computing the stochastic CRB. One of the approaches is computing the asymptotic covariance matrix of the ML estimator and the second one is deriving it directly from extended Slepian-bangs formula. In low DOA estimation and SNRs, the differences between non-circular and circular complex Gaussian CRB are quite important [31]. The CRB is a lower limit on the variance of any unbiased estimator and therefore an important tool to determine the achievement of parameter estimation methods. In particular, the Cramér-Rao inequality states that the covariance matrix of any unbiased estimator satisfies

$Cov\{\theta(x)\} \geq C$

C is the corresponding CRB matrix. Closed form expression for Cramér-Rao bound have been derived. The most preferred among these is the deterministic CRB. Which assumes that the symbols are unknown but can be determined [53].

The angles of direction finding are reduced if two legs of an L-shaped array are not totally upright. The reduction is computed via deterministic CRB. L-shaped data model consists of L_x and L_y number of similar sensors that are equally spaced. The two legs are assumed to share the same sensor at the origin of the Cartesian plane. The Fisher information matrix (FIM) has a (t, u)-th entry equal to [23],

$$[F(\boldsymbol{\xi})]_{t,u} = 2Re\left\{\left[\frac{\partial \boldsymbol{\mu}(\alpha,\beta)}{\partial \xi_t}\right]^H [\Gamma(\alpha,\beta)]^{-1}\left[\frac{\partial \boldsymbol{\mu}(\alpha,\beta)}{\partial \boldsymbol{\xi}_u}\right]\right\} + \mathrm{Tr}\left\{[\Gamma(\alpha,\beta)]^{-1}\left[\frac{\partial \Gamma(\alpha,\beta)}{\partial \boldsymbol{\xi}_t}\right][\Gamma(\alpha,\beta)]^{-1}\left[\frac{\partial \Gamma(\alpha,\beta)}{\partial \boldsymbol{\xi}_u}\right]\right\}. \quad (2.14)$$

Using equation (2.14) the CRBs are given by

$$\begin{bmatrix} CRB(\alpha) & * \\ * & CRB(\beta) \end{bmatrix} = \begin{bmatrix} F_{\boldsymbol{\alpha},\boldsymbol{\alpha}} & F_{\boldsymbol{\beta},\boldsymbol{\alpha}} \\ F_{\boldsymbol{\alpha},\boldsymbol{\beta}} & F_{\boldsymbol{\beta},\boldsymbol{\beta}} \end{bmatrix}^{-1} = \begin{bmatrix} \frac{1}{F_{\boldsymbol{\alpha},\boldsymbol{\alpha}}} & 0 \\ 0 & \frac{1}{F_{\boldsymbol{\beta},\boldsymbol{\beta}}} \end{bmatrix}. \quad (2.15)$$

where $*$ are off diagonal terms.

Using the above approach, the CRBs of the unknown parameters is given by

$$CRB\ (\boldsymbol{\alpha}) = \frac{1}{F_{\boldsymbol{\alpha},\boldsymbol{\alpha}}} \frac{3\,\sigma_c\lambda^2}{4\sigma_s\pi^2 K}\left[\frac{\sin^2(\alpha)}{\Delta_y^2 L_y(L_y-1)(2l_y-1)} + \frac{\cos^2(\alpha+\beta)}{\Delta_x^2 L_x - 1(2L_x-1)}\right]\frac{1}{\theta}. \quad (2.16)$$

$$CRB\ (\boldsymbol{\beta}) = \frac{1}{F_{\boldsymbol{\beta},\boldsymbol{\beta}}} \frac{3\,\sigma_c\lambda^2}{4\sigma_s\pi^2 K}\left[\frac{\cot^2(\alpha)\cos^2\beta}{\Delta_y^2 L_y(L_y-1)(2l_y-1)} + \frac{[\cot(\alpha)\sin(\beta+\alpha)-\sin(\alpha)]}{\Delta_x^2 L_x - 1(2L_x-1)}\right]\frac{1}{\theta}. \quad (2.17)$$

A small wave along the β coordinate is introduced in the CRB(α). The wave becomes more prominent, as the elevation angle α approach 90 degrees. CRB(β) obtain a new peak as elevation angle approaches 90 degrees [32].

A simple statistical data model is used in the analysis of sensor complex gain. Suppose that a sinusoidal signal $z(m)$ at a frequency f_0 and wavelength λ, arriving onto a tetrahedral array from an azimuth angle of $\theta \in [0, 2\pi]$ and an elevation angle of $\theta \in \left[0, \frac{\pi}{2}\right]$. The m^{th} sensor has a array manifold vector equal to [22]

$$\boldsymbol{a}_m = j_m exp\left\{i\frac{2\pi}{\lambda}[x_m \sin(\theta)\cos(\phi) + y_m \sin(\theta)\sin(\phi) + z_m \cos(\theta)]\right\}. \quad (2.18)$$

The tetrahedral array at m^{th} discrete time instant has a 4×1 data vector

$$z(m) = \boldsymbol{a}\sigma_s e^{i(2\pi f_0+\varphi)} + n(m). \quad (2.19)$$

Let take into consideration a linear array sensor with M sensors that are equally spaced. Suppose that there are narrowband signal sources (K). Assume that the incident signal and the noise are uncorrelated. The number of sources is assumed to be less than the number of sensors. The array manifold vector is

$$\boldsymbol{a} = \boldsymbol{e}^{i\left(\frac{2\pi}{\lambda}\boldsymbol{d_1}\sin(\boldsymbol{\theta_k})\right)}. \quad \textbf{(2.20)}$$

The signal assembled by all the sensors at time t can be expressed as

$$Z(t) = As(t) + n(t), \quad (2.21)$$

where $Z(t) = [z_1(t), z_2(t) \ldots z_m(t)]^T$ is a vector received by the array of sensor, A is a array manifold vector $s(t)$ is the signal [16]. A signal source is placed in the far field and emits a sinusoidal signal of

$$z(m) = \sigma_s \exp\left\{i\frac{2\pi c}{\lambda}T_m + \varphi\right\}, \quad (2.22)$$

At the m^{th} time instant, with σ_s known amplitude, a known wavelength of λ, a known speed c and T is the known discrete time sample. The signal arrives upon a dipole triad placed at a spherical coordinates origin. The impinging signal is corrupted by additive noise. The scalars $\varepsilon = \theta, \phi, \gamma, \eta$ are modelled as prior unknown but deterministic. At each time instant m, the dipole triad would collect an $M \times 1$ vector data

$$z(m) = ge^{(\theta,\phi,\gamma,\eta)}\text{s(m)+Jn(m)}. \quad (2.23)$$

Direction of arrival estimation aims to estimate the azimuth angle and the elevation angle, based on the observation [54]. A general case where the azimuth-elevation angle for DOA estimation is considered. Suppose that $F(\varepsilon)$ denotes the Fisher information matrix. Its (k, r) entry is equal to

$$[F(\boldsymbol{\xi})]_{k,r} = 2Re\left\{\left[\frac{\partial \boldsymbol{\mu}}{\partial \xi_k}\right]^H [\Gamma]^{-1}\left[\frac{\partial \boldsymbol{\mu})}{\partial \xi_r}\right]\right\} + \mathrm{T}r\left\{[\Gamma]^{-1}\left[\frac{\partial \Gamma}{\partial \boldsymbol{\xi}_k}\right][\Gamma]^{-1}\left[\frac{\partial \Gamma}{\partial \xi_u}\right]\right\}, \quad (2.24)$$

where $\boldsymbol{\mu} = E[z] = s \otimes ge(\theta, \phi, \gamma, \eta)$, (2.25)

$$\Gamma = \mathrm{E}[(z - \boldsymbol{\mu})(z - \boldsymbol{\mu})^{\mathrm{H}}]\,. \quad (2.26)$$

Since the mean of the equation (2.25) does not depend on the σ_n,it implies that $\frac{\partial \boldsymbol{\mu}}{\partial \sigma_n} = 0$. The covariance matrix of equation (2.24) is independent of $(\theta, \phi, \gamma, \eta)$ implying that

$$\frac{\partial \Gamma}{\partial \theta} = \frac{\partial \Gamma}{\partial \varphi} = \frac{\partial \Gamma}{\partial \gamma} = \frac{\partial \Gamma}{\partial \eta} = 0. \quad (2.27)$$

Thus, the trace of equation (2.24) is equal to zero [54].

The direction of arrival is estimated using nested sparse circular array (NSCA), employing the Cramér-Rao lower bound (CRLB) method. Unknown signal model for NSCA is considered. The CRLB of NSCA is obtained and compared with CRLB of the uniform circular array. CRLB for NSCA is better as compared to the CRLB of UCA for the unknown direction of arrival estimation [9]. A single sensor is used to evaluate the achievement of DOA estimation using CRB method. The sensor is moved to a distinct position to form a virtual sensor array. An inertial measurement unit is used to determine the sensor position and to lower the cost of DOA estimation. CRLB is computed for both the known position of the sensors and when the position is estimated. Using these two approaches, the increase in the sensors does not give important enhancement in the achievement of DOA estimation [33].

The CRB technique is used to estimate the azimuth and elevation angle, of a far-field source using 3D planar array model. CRB expression of a 3D planar array for the conditional and unconditional model is derived and compared with a 2D planar array. When an appropriate rate is selected, a 3D array has superior estimates as compared to 2D planar array for both the azimuth and elevation [33]. Cramér-Rao bound method is used to determine the direction of arrival using lens embedded sensors array. CRLB for DOA estimation is influenced by the angle of arrival and the quality of the lens. The quality of the lens is described by the distance between the center of the lens and the focus [34].

The CRB of direction finding for the lens is given by equation

$$CRB(\phi) = \frac{6\sigma_n^2}{d^2 M(M-1)k^2 h^2 \cos(\phi)}. \tag{2.28}$$

The results above, show that the lens antennae provide better achievement as compared to antennae without the lens [34]. CRB is used as a standard in the assessment of the accuracy of an estimator since its estimate can be evaluated for various practice settings and it is an important tool for practical design [8]. The CRB is obtained from the inverse of the Fisher information matrix [32].

Maximum likelihood (ML) technique is used to estimate the direction of arrival estimation using a uniform linear array. The CRB is used to give a lower bound on the covariance matrix of any unbiased estimator. The ML performance is compared with MUSIC, ESPRIT, and MVDR and evaluated against the CRB. ML estimator exhibit better achievement measure as compared to the other methods [10]. ML estimates the direction of arrival from an array of sensors by maximizing the log-likelihood function. The ML method offers high performance but is computationally expensive [10].

Deterministic and the proposed stochastic ML estimators are compared. The proposed stochastic ML estimators provide better accuracy than deterministic estimator. This method tries to find the parameter values that are most likely to have generated the observed distribution. Maximum likelihood algorithms were among the first algorithms to be scrutinized for direction finding estimation. At low SNR conditions, ML techniques are superior as compared to other estimators. These techniques play an important role in sensor array processing since they give an excellent a trade-off between asymptotic and threshold of estimation achievement. Maximum likelihood is used to estimate the direction of arrival of narrowband signals using scattered sensor arrays [15].

Two-dimensional state-space balance method is used to estimate the direction of arrival employing URA geometry. A far-field wave impinges on the array of the sensors, where the emitter locations are scattered. This method shows better achievement by using discernibility and manageability matrices. This technique gives self-regulating paired 2D direction cosine estimates without an identical pair [33]. Multiple signal classification (MUSIC) and improved Multiple signal classification are used to estimate the direction of arrival estimation using a uniform linear array. The MUSIC technique is inefficient in approximating the impinging coherent signals while the improved version overcomes this problem. Array signal processing strengthens the important signals that impinge on the array of sensors [26]. Planar antenna arrays, including circular, concentric and hexagonal, rectangular and V-shaped are used to estimate the problem of DOA using super-resolution MUSIC method. The false peaks problem that occurs in the spatial spectrum is also considered. The achievements are determined in various noise environments. The more the

opening the less probability for a false peak to occur. It was established that rectangular array is the most vulnerable in producing false peaks while V-shaped is the least [35].

The MUSIC technique is based on the eigen decomposition of the covariance matrix of the received signal. It gives higher ranking resolution since it has essential eigen structure. It executes well in case of incoherent signals, but its performance reduces in signals having the same phase and frequency [35]. DOA estimation problem is considered using circular and concentric circular arrays, employing MUSIC technique. The problem of measuring the incorrect peak is also taken into consideration. To conquer the problem of DOA estimation, azimuth and elevation angles are estimated. A narrowband signal $s(t) = \mathrm{u(t)}\cos[\omega_0 + \mathrm{v(t)}]$ is considered. Concentric antennae array comprising of two circular arrays, with three and four sensors respectively. Two signals impinge at the array of the sensor at azimuth and elevation angles $\beta_1 = 20^0, \alpha_1 = 20^0, \beta_2 = 45^0, \alpha_1 = 45^0$. Multiple incorrect peaks occur around the verified mesh of the sources of the signals. The number of incorrect peaks taking place in the concentric array is higher as compared to a circular array [25].

Concentric circular arrays (CCAs) is used to estimate the DOA estimation problem using MUSIC technique, and it compared to ULA and UCA. The central point of the array is taken as the reference point. The position of the last sensor is $r_g = (r_g \cos(\beta_g), r_g \sin(\beta_g), 0)$. ULA can only estimate azimuth angle, while CCAs estimate azimuth and elevation angles. CCAs gives a more precise estimation as compared to ULA and UCA for higher angles resolutions. Higher computational power is required in approximating the DOA in CCA as contrasted to ULA and UCA [17].

MUSIC is used to estimate direction of arrival estimation. In the last decades, wireless communication services have increased rapidly. The significance factor of research in wireless communication have increased the demand for the improvement of the capacity, coverage and quality of communication systems. There are many factors that affect the performance of MUSIC, they include the number of sensors, number of snapshot and inter-sensor spacing. The simulation results show that when the number of snapshot increases,

the accuracy of DOA estimation increase. When the number of array of sensors increases, the accuracy increases but the speed decreases. When the inter-sensor spacing is less than half wavelength, the MUSIC technique resolution improves [22].

DOA estimation is estimated using L-shaped array employing Tayem's algorithm and Kikuchi's algorithm, these methods estimate the azimuth and elevation angles of arrival, by an extended performance of cross-correlation matrix obtained from an L-shaped. Azimuth angles are obtained by the interrelation between the elevation and azimuth angle. At small signal-to-noise ratio and with a low number of snapshots, Tayem's algorithm and Kikuchi's algorithm gives better achievement as compared to MUSIC and ESPRIT methods [36]. MUSIC and ESPRIT are alike in that they exploit the fundamental data model and initiate estimates that are asymptotically unbiased. ESPRIT has lower computational complexity and the requirements for storage are lower than MUSIC.

2.3 Comparison of the performance

This section compares the variables of the circular, octagonal, hexagonal, and rectangular arrays employing MUSIC technique method. Also, hexagonal array and circular array are compared using improved swarm optimization method and uniform and non-uniform array have been compared in direction finding using MUSIC to demonstrate the performance of the proposed geometries.

Circular, octagonal, hexagonal and rectangular antennas arrays are compared in DOA estimation using super-resolution method MUSIC. The signal sources on the azimuth and polar angle were estimated by sensors. The octagonal array has a slightly higher root mean square error (RMSE) of MUSIC as compared to the other geometries while hexagonal array has the highest RMSE thus poor DOA accuracy. The rectangular arrays can have the lowest RMSE thus highest accuracy if they never had many false peaks on the spatial spectrum [37]. Circular, hexagonal and octagonal array for smart antennae are compared using global hybrid optimization method. Central force optimization and hill climbing algorithm are combined. The comparison between the geometries indicated that hexagonal array gave slightly deeper nulls and higher gain with respect to circular and octagonal arrays. Uniform

hexagonal array had a small overall size with the same beam width as compared to circular and octagonal array [38].

Hexagonal and circular antennae array employing improved swarm optimization method using identical antennae is compared. For comparison purpose, two different optimization problems where circular antennae and hexagonal antennae comprise 12 and 18 elements are considered. The number of the antennae array is reduced from 12 to 6 using improved swarm optimization method. Hexagonal antennae exhibit superior achievement as compared to circular antennae [39]. Circular, pyramid, slant, spiral, dual-circular and planar arrays for two-dimensional DOA estimation have been compared using MUSIC. The geometries performance is compared based on the CRB. When the polar angle is close to 0 degrees, the CRB of the polar angle is incompletely poor for the UCA. Thus, the polar reduces when the waveforms are moving from the horizon. The CRB for the polar angle for the other geometries has no asymptotical characteristic, implying that the polar angle estimation is performance is improved. The best accuracy is achieved for the planar array when the elevation angle is at 90 degrees [40].

MUSIC and ESPRIT of DOA estimation techniques are compared using Kalman filter. The tracking is conducted out starting from DOA estimation. The DOA is considered as an initial value, the Kalman filter is used to track the source in motion based on the motion model. The comparison is made in terms of signal-to-noise ratio, number of snapshots and the number of sensor arrays. The ESPRIT algorithm was highly accurate and acted as the best initial estimate for Kalman filter tracking algorithm [41].

Hexagonal arrays are broadly used in the enactment but have obtained less attention in array signal processing. Unitary ESPRIT is applied to hexagonal array for the direction of arrival estimation. This technique gives a computationally systematic DOA estimation. The mean square error is close to the CRB and threshold behavior is perfect [12]. Directive antennas in uniform circular arrays are used to estimate the direction of arrival. The CRLB of UCA is derived with directional antennas and is compared to an identical sensor for 4 and 8 elements arrays. The directivity that reduces the CRB is distinguished and microstrip

patch elements estimating the optimal theoretical gain pattern are sketched, to compare direction finding accuracy with UCA using dipole elements. The improved DOA was acquired with suitable directivity [19].

A comparative study was conducted of direction finding using uniform and non-uniform linear array employing MUSIC method. The non-uniform array had superior estimation as compared to a linear array which resulted in expanding the wireless capacity. A sensor is a group of sensors deployed in a certain geometry pattern, used for collecting and processing electromagnetic or acoustic signals [16]. Employing an array of sensors has an advantage over a single sensor in attaining achievement for better accuracy estimation. The enhanced achievement involves depletion of the interference from a certain direction and determining the direction of arrival of the impinging signals [16].

MUSIC technique is used to determine the direction of arrival using a uniform circular array [6]. MUSIC based on UCA is compared to MUSIC based on ULA. MUSIC based on UCA is the most appropriate in airborne DOA estimation system. Since it is simple to plan and also the coherent signals do not depend on the aerial reflector around the sensors. Array signal processing (ASP) is a new algorithm in Digital Signal Processing with many applications [14]. DOA estimation for ULA using the MUSIC and ESPRIT techniques is determined. Identical sensors are linearly distributed on the ULA. The techniques give accurate DOA estimation than classical techniques. The achievement of these techniques improves when the number of sensors on the array increases [41].

UCA is used to determine the direction of arrival using the MUSIC method. It compares direction finding of identical elements with that of non-identical elements. To achieve this, the CRLB for both geometries of identical and nonidentical elements is derived. The CRLB for the azimuth angle of the UCA employing identical elements is given as

$$\mathrm{CRLB}(\varphi) = \frac{2\sigma^2\alpha^{-1}\left|\left|\mathrm{b}(\theta)\right|\right|^2}{4\left|\left|\mathbf{b}(\theta)\right|\right|^2\left|\left|\left(\frac{\partial \mathbf{b}}{\partial \theta}\right)^2+\left|\left|\left(\frac{\partial \mathbf{b}}{\partial \theta}\right)^{\mathrm{H}}\mathbf{b}(\boldsymbol{\theta})-\mathbf{b}^{\mathrm{H}}\left(\frac{\partial \mathbf{b}}{\partial \theta}\right)\right|\right|^2-\left|\left|\left(\frac{\partial \mathbf{b}}{\partial \theta}\right)\right|\right|^2}. \quad (2.29)$$

The above CRLB indicate that accurate DOA estimation can be achieved using

identical elements [19].

Uniform linear array and non-uniform linear array are used to estimate DOA using MUSIC algorithm. This algorithm determines factors that influence the precision of direction finding. When the number of sensors and the signal-to-noise ratio is high, this technique gives better estimates. Non-uniform linear array gives accurate estimates as compared to a uniform linear array. Non-uniform linear array assists to obtain better estimates of DF which result in enhancement of wireless communication system [35]. Planar and volume arrays with isotropic sensor have been used for direction of arrival estimation performance. For planar arrays, the array is identical since the CRB of the DOA estimation of a single source is uniform for the angles of arrival. The array of sensors is said to be isotropic if the bound on the mean square error (MSAE) is constant for all the azimuth and polar angles. The necessary and sufficient conditions of the geometry were derived that ensured that the MSAE is not independent on the source azimuth and polar angles. The azimuth and polar angles are uncoupled in the CRB, and the CRB is not dependent on the signal arrival angle when the conditions are satisfied [43].

Automotive radar sensors arrays are used to estimate DOA estimation using narrowband technique. The automotive radar is used in advance driver assisted systems. The systems are used to estimate the position of the objects. Bartlet, capon, and MUSIC techniques were compared to narrowband technique. The narrowband technique had a smallest DOA estimation error. This method formed no side lobes and very sharp main lobes. The narrowband technique had the better achievement than conventional algorithm in terms of DOA estimation and resolution [44].

Cramér-Rao bound and root means square error (RMSE) are used as theoretical tools to analyze the performance of MUSIC, R-MUSIC and ESPRIT technique in DOA estimation. Analysis of Uniform circular array (UCA), L-shaped array (LSA), double L-shaped array (DLSA) and double uniform circular array (DUCA) is demonstrated. Considering both azimuth and elevation estimation LSA and DLSA are more accurate as contrasted to others. MUSIC is more accurate as compared to the other techniques [46]. The achievement of

different parameter estimation techniques in DOA using linear array with inter-sensor spacing being more than half the wavelength is studied. Beamformer methods, MUSIC, ESPRIT, and Space-Alternating Generalized Maximization-expectation (SAGE) trigger an ambiguous error in the results of the estimated DOA, when the inter-sensor spacing is more than half the wavelength [46].

Planar arrays and volume arrays are used to estimate the accuracy of direction of arrival, using MUSIC method for electronic surveillance measure (ESM). The achievement of the arrays is compared depending on root mean square error, ambiguity function, and CRB. Depending on RMSE, CRB, and array ambiguity the planar arrays have better accuracy of DOA estimation, as compared to volume arrays [47]. R-Music technique is used to determine the DOA estimation using virtual UCA and compares it with classical MUSIC. CRB is derived to determine the accuracy of DOA estimation. From the result, R-MUSIC is more accurate as compared to classical MUSIC [48].

DOA estimation is not only affected by the incoming signal from the source but also by the scanty complex environment. It is affected by many factors such as signal-noise-ratio, number of sensors, number of snapshots, and number of signal sources [16]. The signal-to-noise ratio (SNR) is a measure used in science and engineering that compares the level of the desired signal to the level of background noise. It can be strengthened by using the source with higher signal output power if required [19]. It directly influences the achievement of super-resolution direction finding algorithms. Super-resolution algorithms performance drops suddenly when the SNR lowers.

A number of snapshots are defined as the number of samples in the time domain. In the frequency domain, it is defined as the number of time sub-segments of discrete Fourier transform. As a result of direction finding the higher the number of snapshots, the better the estimation achievement for techniques when the other parameters are held constant [49]. It refers to the signal conveyed from the transmitter to the receiver [16]. As the number of the array of sensors increases, MUSIC can correctly determine the DOA of the

incoming signals. When the number of sensors reduces, the resolution of MUSIC techniques reduces [50]. Mutual coupling between the sensors manipulate the array output signal and lowers the achievement of DOA estimation. ESPRIT method gives a more stable and accurate estimate of mutual coupling. It indicates that better estimation performance is achieved under small snapshot [51].

An antenna array is a set of multiple connected antennae which work together as a single antenna, to transmit or receive radio waves [16]. The preferred signals from the sensors are joined and processed in order to acquire an improved achievement over a single sensor. An array of sensors has advantages over a single sensor of obtaining an improved achievement when employing MUSIC techniques [52]. An array of sensors can be arranged in a different pattern to yield a different ray's pattern. Some of the typical array geometries arrays include Linear array, whereby the sensor are placed along a straight line with equal inter-sensor spacing between any two adjacent sensors. Non-linear array, whereby the sensor array elements arranged along a straight line with a non-equal spacing distance between two adjacent sensor elements and phase difference. Circular array, whereby the sensor array elements are arranged around the circumference of a circle. Planar array, whereby the sensor array elements are arranged over some planar surface [16].

CHAPTER THREE

METHODOLOGY

This chapter deals with the description of the procedures followed while achieving the following objectives array manifold vector for the uniform hexagonal array, Cramér-Rao bound for the uniform hexagonal array as well as comparing the derived Cramér-Rao bound for UHA with that of UCA. The steps for deriving the array manifold vector and Cramér-Rao bound for the UHA are outlined. Finally, comparison procedures for the Cramér-Rao bound for UHA and UCA are reviewed.

3.1 Derivation of the array manifold vector for the uniform hexagonal array (UHA)

In this section, the uniform hexagonal array geometry has been described and the steps for deriving its array manifold vector outlined.

It is the set of array responses of a signal for all possible azimuth-polar angles. To be able to estimate azimuth- polar angles of a signal, knowledge of the array manifold vector is required.

The starting point for determining the direction of arrival estimation is the definition of the array manifold vector. It is sampled over a Grid of polar and azimuth angles defined by θ and ϕ respectively. A hexagon of edge length R centered at the Cartesian origin and lying on the x-y plane was considered. M number of isotropic sensors were uniformly distributed on the circumference of the hexagon, with equal inter-sensor spacing. A complex-valued incident signal from a far-field source impinged on an array of sensors at an azimuth angle ϕ, which was measured counterclockwise from the positive x-axis and a polar angle θ, measured clockwise from the positive z-axis as shown below,

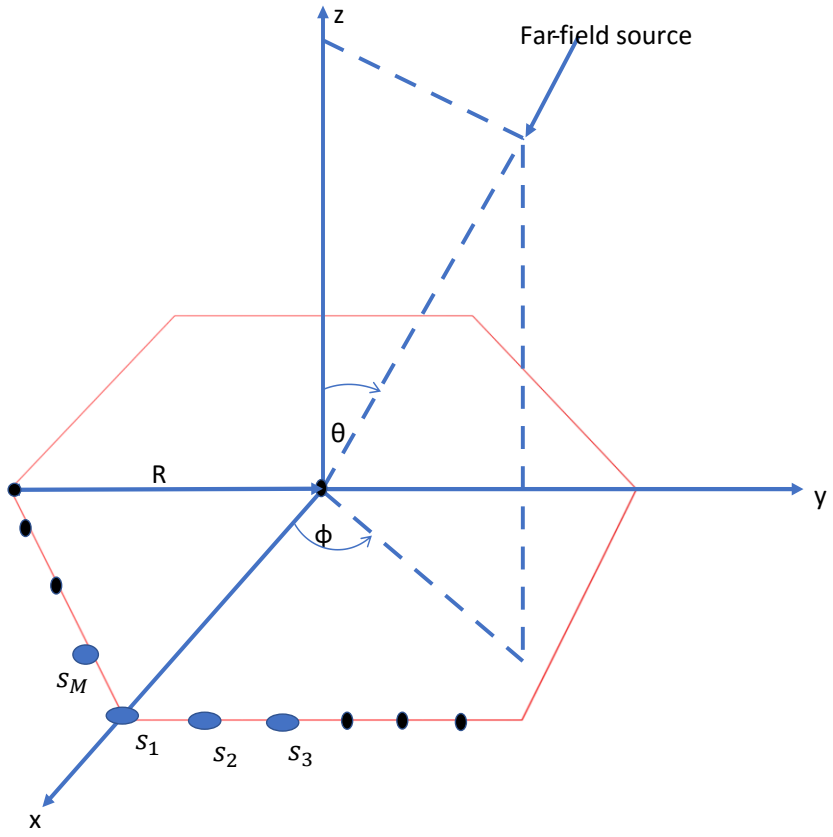

Figure 3. 1: Uniform hexagonal array

The following steps were followed in order to achieve this objective;

3.1.1 Location of the general position of the sensors

Using the procedure of deriving the array manifold of the ULA, the array manifold for UHA was derived. The general location of the sensors that were uniformly distributed on the hexagon, were expressed in terms of the polar coordinate system. It was assumed that suppose ℓ number of the sensors were uniformly distributed on the UHA with equal inter-sensor spacing for ℓ = 1,2,3..., L. The general position of the ℓ^{th} element position was given by equation below,

$$\boldsymbol{p}_{\ell} = \left[x_l cos\left(\frac{2\pi(\ell-1)}{L}\right),\ x_l sin\left(\frac{2\pi(\ell-1)}{L}\right),\ 0\right]^T, \tag{3.11}$$

where x_l denotes the general distance from the origin of a cartesian coordinate system to any sensor, T is the transpose and L is the total number of sensor.

3.1.2 Determination of the observations received at the array of sensor

Observations received at the array of sensors were determined based on the information received by each sensor. It was assumed that suppose $g(t)$ is the signal received at the origin of a Cartesian coordinate system, then the observations at the array of sensors of a UHA is given as

$$\mathbf{g}(t,p)=\begin{Bmatrix} g(t-\tau_1) \\ g(t-\tau_2) \\ \vdots \\ g(t-\tau_L) \end{Bmatrix} \tag{3.12}$$

where $\mathbf{g}(t,p)$ is the observations at the array of sensors, τ is the time delay and t is time.

$$\tau = \frac{\omega(\theta,\phi)^T \mathbf{P}_\ell}{c}. \tag{3.13}$$

c is the velocity of light, $\mathbf{p}_\ell$ is position vector of a sensor general position. The direction of plane wave propagation in unit direction was to be given as

$$\mathbf{w}(\theta,\phi) = \begin{bmatrix} \cos(\theta) \\ \sin(\theta) \end{bmatrix}. \tag{3.14}$$

Combining equation (3.13) and (3.14)

$$\tau_l = -\frac{1}{c}\left[p_{x_l}\cos(\theta) + p_{y_l}\sin(\theta)\right] = \frac{[x_l\cos(\theta) - y_l\sin(\theta)]}{c}. \tag{3.15}$$

3.1.3 Conversion of time domain signal into frequency domain signal

Time domain signal was converted into a frequency domain signal, by taking the Fourier transform (FT) of the observations that were received at the array of sensors. Consider conversion of a time domain signal to frequency domain signal of a UHA

$$\boldsymbol{G}_\ell(\omega) = \int_{-\infty}^{\infty} e^{-i\omega t}\, g(t-\tau_\ell)dt = \boldsymbol{G}(\omega)e^{\left\{\frac{i\,2\,\pi}{\lambda}[x_l\cos(\theta)+y_l\sin(\theta)]\right\}}. \tag{3.16}$$

where λ is the wavelength, $\omega = 2\pi f$ is angular frequency, $\boldsymbol{G}_\ell(\omega)$ is the frequency domain signal of the ℓ^{th} sensor.

All the sensors were assumed to be identical and thus their frequency response was the same. Sensor output vector was expressed in terms of a frequency domain to reduce the level of Gaussian noise. Hence,

$$\boldsymbol{G}(\omega) = \begin{bmatrix} G_1(\omega) \\ G_2(\omega) \\ G_3(\omega) \\ \vdots \\ G_L(\omega) \end{bmatrix} = \boldsymbol{G}(\omega) \begin{bmatrix} \exp\left\{\frac{i\,2\pi}{\lambda} x_0 \cos(\theta) + y_0 \sin(\theta)\right\} \\ \exp\left\{\frac{i\,2\pi}{\lambda} x_1 \cos(\theta) + y_2 \sin(\theta)\right\} \\ \exp\left\{\frac{i\,2\pi}{\lambda} x_3 \cos(\theta) + y_3 \sin(\theta)\right\} \\ \vdots \\ \exp\left\{\frac{i\,2\pi}{\lambda} x_n \cos(\theta) + y_n \sin(\theta)\right\} \end{bmatrix}. \quad (3.17)$$

where $l = 1,2,3 \ldots L$.

The observations in frequency domain consists of the scalar and complex part, since the scalar part was constant the array manifold was to be given by the complex part.

$$\mathbf{a} = \begin{bmatrix} \exp\left\{\frac{i\,2\pi}{\lambda} x_0 \cos(\theta) + y_0 \sin(\theta)\right\} \\ \exp\left\{\frac{i\,2\pi}{\lambda} x_1 \cos(\theta) + y_2 \sin(\theta)\right\} \\ \exp\left\{\frac{i\,2\pi}{\lambda} x_3 \cos(\theta) + y_3 \sin(\theta)\right\} \\ \vdots \\ \exp\left\{\frac{i\,2\pi}{\lambda} x_n \cos(\theta) + y_n \sin(\theta)\right\} \end{bmatrix}. \quad (3.18)$$

Array manifold vector for uniform circular array (UCA)

A circle of radius *R* centered at the Cartesian origin and lying on the *xy*-plane was considered as shown below,

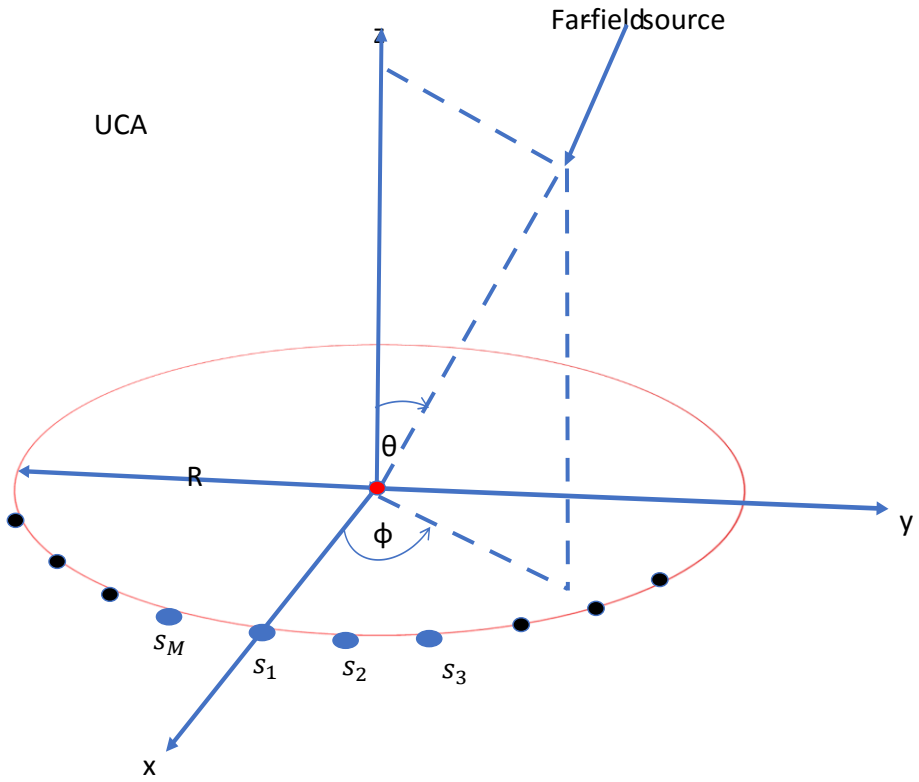

Figure 3. 2: Uniform circular array

In the figure above, *M* number of sensors were uniformly distributed along the circumference of the circle of radius *R*. The central point of the array was at the origin of a Cartesian coordinate system. The sensor located at the positive *x*-axis was denoted as $s_1$while the remaining sensors were uniformly arranged counterclockwise on the circumference of the circle. Plane waves from a far-field source impinged on the sensors at an azimuth angle of ϕ, measured counterclockwise from the positive *x*-axis and a polar angle θ, measured clockwise from the positive *z*-axis.

The position of the sensors for $m = 1,2,3, \dots, M$ was generally given by

$$\boldsymbol{p}_m = \left[R\cos\left(\frac{2\pi(m-1)}{M}\right), R\ \sin\left(\frac{2\pi(m-1)}{M}\right), 0\right]^T \quad (3.19)$$

and $\frac{2\pi R}{L}$ was the angular distance between any two consecutive sensors. Suppose that $y(t)$ was the signal that was received at the origin of the Cartesian coordinate system at time t, then the observations at the array of sensors was given by

$$\boldsymbol{y}(t,\boldsymbol{p}) = \begin{bmatrix} y(t-\tau_1) \\ y(t-\tau_2) \\ \vdots \\ y(t-\tau_M) \end{bmatrix}, \tag{3.20}$$

where $\mathbf{p}_\mathrm{m} = \boldsymbol{p_1}, \mathbf{p}_2, \mathbf{p}_3 \ldots \mathbf{p}_{\boldsymbol{M}}$, $\tau_m = \frac{v(\theta,\phi)^T \boldsymbol{p}_m}{c}$ and

$$v(\theta,\phi) = -\begin{bmatrix} v_x(\theta,\phi) \\ v_y(\theta,\phi) \\ v_z(\theta) \end{bmatrix} = -\begin{bmatrix} \sin(\theta)\cos(\phi) \\ \sin(\theta)\sin\phi \\ \cos(\theta) \end{bmatrix}. \tag{3.21}$$

$v_x(\theta,\phi)$, $v_y(\theta,\phi)$ and $v_z(\theta)$ are the direction cosines along x, y and z axes respectively.

To convert the time domain signal into the frequency domain signal, Fourier transform of $\mathbf{y}(\mathrm{t},\mathbf{p})$ was taken

$$Y_m(\omega) = \int_{-\infty}^{\infty} y(t-\tau_m)e^{-i\omega t}dt \;\; = Y_m(\omega)e^{-i\omega\tau_m}, \tag{3.22}$$

where $\omega = 2\pi f$.

Therefore, we have the frequency domain observations as

$$Y(\omega) = \begin{bmatrix} Y_1(\omega) \\ Y_2(\omega) \\ \vdots \\ Y_L(\omega) \end{bmatrix} = Y(\omega)\begin{bmatrix} \exp\left\{i\frac{2\pi R}{\lambda}\sin(\theta)\cos(\phi)\right\} \\ \exp\left\{i\frac{2\pi R}{\lambda}\sin(\theta)\cos(\phi-\frac{2\pi}{L})\right\} \\ \exp\left\{i\frac{2\pi R}{\lambda}\sin(\theta)\cos(\phi-\frac{4\pi}{L})\right\} \\ \vdots \\ \exp\left\{i\frac{2\pi R}{\lambda}\sin(\theta)\cos\left(\phi-\frac{2\pi(L-1)}{L}\right)\right\} \end{bmatrix}. \tag{3.23}$$

The array manifold was thus given by the complex-valued vector since the $Y(\omega)$ was a constant and hence can be ignored.

$$\boldsymbol{a}_{\mathrm{UCA}} = \begin{bmatrix} \exp\left\{i\frac{2\pi R}{\lambda}\sin(\theta)\cos(\phi)\right\} \\ \exp\left\{i\frac{2\pi R}{\lambda}\sin(\theta)\cos(\phi-\frac{2\pi}{L})\right\} \\ \exp\left\{i\frac{2\pi R}{\lambda}\sin(\theta)\cos(\phi-\frac{4\pi}{L})\right\} \\ \vdots \\ \exp\left\{i\frac{2\pi R}{\lambda}\sin(\theta)\cos\left(\phi-\frac{2\pi(L-1)}{L}\right)\right\} \end{bmatrix}. \tag{3.24}$$

3.2 Derivation of the Cramér-Rao bound for UHA

The following steps were followed in the derivation of the Cramér-Rao bound for the uniform hexagonal array;

3 .2.1 Data model

To focus on the estimation of the direction of arrival, a statistical model was assumed based on the array manifold vector, incident signal and the noise [36],

$$\mathbf{z}(\mathbf{m}) = \mathbf{a}\,\mathrm{s(m)} + \mathbf{n}(\mathbf{m}) \qquad m = 1,2,3 \ldots\ldots\ldots\ldots M. \tag{3.25}$$

s(m) is the signal released at time t, **a** is the array manifold vector that correspond to the geometrical pattern under consideration and $\boldsymbol{n}$**(m)** is the noise. The observed data vector followed multivariate normal/Gaussian distribution. For multiple snapshots the data model vector was assumed to be given by [2]

$$\tilde{\boldsymbol{z}} = \boldsymbol{s} \otimes \boldsymbol{a}(\theta, \phi) + \tilde{\boldsymbol{n}} \tag{3.26}$$

Where $\tilde{\boldsymbol{z}} = [\boldsymbol{z}_1, \boldsymbol{z}_2, \cdots, \boldsymbol{z}_M]^T, \boldsymbol{s} = s_1, s_2, \cdots s_M, \boldsymbol{a} = a_1, a_2, \cdots, a_M\ \tilde{\boldsymbol{n}} = [\boldsymbol{n}_1, \boldsymbol{n}_2, \cdots, \boldsymbol{n}_M]^T$

The probability density function of $\tilde{\boldsymbol{z}}$ is given by

$$p(\tilde{\boldsymbol{z}}|\boldsymbol{\theta}) = \frac{\mathbf{1}}{\sqrt{|2\pi\tilde{\boldsymbol{\Gamma}}(\theta,\phi)|}} \exp\left\{-\frac{1}{2}[\tilde{\boldsymbol{z}} - \tilde{\boldsymbol{\mu}}(\theta,\phi)]^H \tilde{\boldsymbol{\Gamma}}(\theta,\phi)^{-1}[\tilde{\boldsymbol{z}} - \tilde{\boldsymbol{\mu}}(\theta,\phi)]\right\}, \tag{3.27}$$

where $\tilde{\boldsymbol{\mu}}(\theta,\phi) = E[\tilde{\boldsymbol{z}}] = \boldsymbol{s} \otimes \boldsymbol{a}(\theta,\phi)$, $\tilde{\boldsymbol{\Gamma}}(\theta,\phi) = E\{[\tilde{\boldsymbol{z}} - \tilde{\boldsymbol{\mu}}(\theta,\phi)][\tilde{\boldsymbol{z}} - \tilde{\boldsymbol{\mu}}(\theta,\phi)]^H\}$.

3.2. 2 Fisher information matrix

Scalar parameters to be estimated were collected as the entries of a vector $\xi = [\theta, \varphi]$. Fisher information matrix (FIM) of (k, r)-th entry is given by,

$$[F(\boldsymbol{\xi})]_{k,r} = 2Re\left\{\left[\frac{\partial \boldsymbol{\mu}}{\partial \xi_k}\right]^H [\Gamma]^{-1} \left[\frac{\partial \boldsymbol{\mu}}{\partial \xi_r}\right]\right\} + \mathrm{T}r\left\{[\Gamma]^{-1}\left[\frac{\partial \Gamma}{\partial \xi_k}\right][\Gamma]^{-1}\left[\frac{\partial \Gamma}{\partial \xi_r}\right]\right\} \tag{3.28}$$

where k, r = [1,2], $\boldsymbol{\xi}_k$is the k^{th} of $\boldsymbol{\xi} = [\boldsymbol{\theta}, \boldsymbol{\phi}]$, Re and Tr denotes the real part and the trace

of the identity inside the curly brackets respectively. The superscript H denotes conjugate transposition.

The elements of the FIM were obtained as follows;

$$[F(\boldsymbol{\xi})]_{1,1} = 2Re\left\{\left[\frac{\partial \boldsymbol{\mu}}{\partial \xi_1}\right]^H [\Gamma]^{-1} \left[\frac{\partial \boldsymbol{\mu}}{\partial \boldsymbol{\xi_1}}\right]\right\} + \mathrm{Tr}\left\{[\Gamma]^{-1} \left[\frac{\partial \Gamma}{\partial \xi_1}\right] [\Gamma]^{-1} \left[\frac{\partial \Gamma}{\partial \boldsymbol{\xi_1}}\right]\right\} \tag{3.29}$$

$$[F(\boldsymbol{\xi})]_{1,2} = 2Re\left\{\left[\frac{\partial \boldsymbol{\mu}}{\partial \boldsymbol{\xi_1}}\right]^H [\Gamma]^{-1} \left[\frac{\partial \boldsymbol{\mu}}{\partial \xi_2}\right]\right\} + \mathrm{Tr}\left\{[\Gamma]^{-1} \left[\frac{\partial \Gamma}{\partial \boldsymbol{\xi_1}}\right] [\Gamma]^{-1} \left[\frac{\partial \Gamma}{\partial \xi_2}\right]\right\} \tag{3.30}$$

$$[F(\boldsymbol{\xi})]_{2,1} = 2Re\left\{\left[\frac{\partial \boldsymbol{\mu}}{\partial \boldsymbol{\xi_2}}\right]^H [\Gamma]^{-1} \left[\frac{\partial \boldsymbol{\mu}}{\partial \boldsymbol{\xi_1}}\right]\right\} + \mathrm{Tr}\left\{[\Gamma]^{-1} \left[\frac{\partial \Gamma}{\partial \xi_2}\right] [\Gamma]^{-1} \left[\frac{\partial \Gamma}{\partial \xi_1}\right]\right\} \tag{3.31}$$

$$[F(\boldsymbol{\xi})]_{2,2} = 2Re\left\{\left[\frac{\partial \boldsymbol{\mu}}{\partial \xi_2}\right]^H [\Gamma]^{-1} \left[\frac{\partial \boldsymbol{\mu}}{\partial \xi_2}\right]\right\} + \mathrm{Tr}\left\{[\Gamma]^{-1} \left[\frac{\partial \Gamma}{\partial \xi_2}\right] [\Gamma]^{-1} \left[\frac{\partial \Gamma}{\partial \xi_2}\right]\right\}. \tag{3.32}$$

where $\boldsymbol{\mu} = E[\hat{z}] = \boldsymbol{s} \otimes \boldsymbol{a}(\theta, \phi)$, $\Gamma = \frac{2}{n}\mathbf{I}_{TM\times TM}$, TM is the tangent bundle of manifold M, $E[\hat{z}]$ is statistical expectation of $\hat{z}$ and $I_{TM\times TM}$ is the identity matrix of size TM. Since Γ is independent of θ and ϕ, then $\frac{\partial \Gamma}{\partial \varepsilon} = 0$.

The fisher information matrix was given by equation

$$\begin{bmatrix} [F(\boldsymbol{\xi})]_{1,1} & [F(\boldsymbol{\xi})]_{1,2} \\ [F(\boldsymbol{\xi})]_{2,1} & [F(\boldsymbol{\xi})]_{2,2} \end{bmatrix}. \tag{3.33}$$

$$\boldsymbol{F}(\boldsymbol{\xi}) = \begin{bmatrix} F_{\theta,\theta} & F_{\theta,\phi} \\ F_{\phi,\theta} & F_{\phi,\phi} \end{bmatrix} \tag{3.34}$$

$$\begin{bmatrix} \mathrm{CRB}(\theta) & * \\ * & \mathrm{CRB}(\phi) \end{bmatrix} = \begin{bmatrix} F_{\theta,\theta} & F_{\theta,\phi} \\ F_{\phi,\theta} & F_{\phi,\phi} \end{bmatrix}^{-1} = \frac{1}{F_{\theta,\theta}F_{\phi,\phi} - F^2{}_{\theta,\phi}} \begin{bmatrix} F_{\phi,\phi} & -F_{\theta,\phi} \\ -F_{\phi,\theta} & F_{\theta,\theta} \end{bmatrix}, \tag{3.35}$$

Where * are off diagonal terms.

Thus, the CRBs for the uniform hexagonal array geometry was obtained using the following formula,

$$\mathrm{CRB}(\theta) = \frac{F_{\phi,\phi}}{F_{\theta,\theta}F_{\phi,\phi} - F^2{}_{\theta,\phi}}, \tag{3.36}$$

$$\mathrm{CRB}(\phi) = \frac{F_{\theta,\theta}}{F_{\theta,\theta}F_{\phi,\phi} - F^2{}_{\theta,\phi}}. \tag{3.37}$$

CRBs for the azimuth and polar angle were obtained from the inverse of the Fisher information matrix.

Using the same procedure for deriving the array manifold and Cramér-Rao bound of the UHA, the array manifold and CRB for the UCA were derived.

3.3 Comparison of the Cramér-Rao bound of uniform hexagonal array and that of uniform circular array

In this section, the Cramér-Rao bound of the uniform hexagonal array is compared with Cramér-Rao bound of the uniform circular array using the ratio method. The performance comparison considers the accuracy of the DOA estimation which is the most important factor of the performance since it designates the estimation accuracy. The ratio of CRB of the UHA to the corresponding CRB of UCA was obtained. The ratio was analyzed into three possible scenarios, when the ratio was less than one when the ratio was equal to one and finally when the ratio was greater than one. The results were validated through Graphical representation.

CHAPTER FOUR

RESULTS AND DISCUSSION

In this chapter, a two-dimensional array manifold vector and Cramér-Rao bound for the UHA were derived. The derived Cramér-Rao bound for the UHA is compared with the Cramér-Rao bound for the UCA using the ratio method.

4.1 Derivation of Array Manifold Vector for the Uniform Hexagonal Array (UHA)

In this section a general distance from the reference point of the hexagon to any sensor was obtained, the general position of the sensors was attained, the time delay for the signal to arrive at the last sensor was derived, time domain signal was converted into frequency domain signal and finally the observations in the frequency domain signal gave the array manifold vector for uniform hexagonal array.

To describe the array manifold vector of a complex valued signal impinging on the uniform hexagonal array of sensors, the general distance from the center of an equilateral triangle of a hexagon to any sensor was given by

$$x_k = \frac{R}{2}\sqrt{3 + \left[\frac{2k-1}{n-1}\right]^2}, \tag{4.11}$$

Where n is even number of sensors in an equilateral triangle and $k = 1,2,3 \ldots \frac{n}{2}$.

Substituting equation (4.11) into equation (3.11) the location of the m^{th} sensor was given by

$$\boldsymbol{P_m} = \left[x_k cos\left(\frac{2\pi(m-1)}{M}\right), x_k sin\left(\frac{2\pi(m-1)}{M}\right),\ 0\ \right]^T \tag{4.12}$$

where $m = 1,2, \ldots M$ and M denotes the total number of sensor.

Observations received at the array of sensors was determined based on the information received by each sensor,

$$y(t, \boldsymbol{p}) = \begin{Bmatrix} y(t-\tau_1) \\ y(t-\tau_2) \\ \vdots \\ y(t-\tau_M) \end{Bmatrix},$$

where $\boldsymbol{p} = \boldsymbol{p}_1\, \boldsymbol{p}_2 \ldots \boldsymbol{p}_M$ is the general position of the $m^{th}\ sensor$ and

$$\tau_M = \frac{v(\theta,\phi)^T \boldsymbol{P}_m}{\mathrm{c}} \tag{4.13}$$

is the time delay for the signal to reach the m^{th}sensor.

In the above

$$v(\theta, \phi) = -\begin{bmatrix} v_x(\theta,\phi) \\ v_y(\theta,\phi) \\ v_z(\theta) \end{bmatrix} = -\begin{bmatrix} sin(\theta)\, cos\, \phi \\ sin(\theta)\, sin(\phi) \\ cos(\theta) \end{bmatrix}, \tag{4.14}$$

where $v_x(\theta,\phi)$, $v_y(\theta,\phi)$ and $v_z(\theta)$ are direction cosines along x, y and z axes, respectively. The negative sign arises due to the direction of the incident signal.

Explicitly, using equation (4.12) and equation (4.14) in equation (4.13)

$$\tau_M = \frac{-1}{\lambda f}[\sin(\theta)\cos(\phi), \sin(\theta)\sin(\phi), \cos(\theta)] \begin{bmatrix} x_k \cos\left(\frac{2\pi(m-1)}{M}\right) \\ x_k \sin\left(\frac{2\pi(m-1)}{M}\right) \\ 0 \end{bmatrix} =$$

$$\frac{x_k \sin(\theta)}{\lambda f} \cos\left(\phi - \frac{2\pi(m-1)}{M}\right). \tag{4.15}$$

To convert the time domain signals into frequency domain, we took the Fourier transform of

y (t, p) from which we got the m^{th} component to be

$$Y_m(\omega) = \int_{-\infty}^{\infty} e^{-i\omega t}\, y(t-\tau_\ell)dt = Y(\omega)e^{-i\omega t}$$

$$= Y(\omega)exp\left\{\frac{i2\pi x_k}{\lambda}\sin(\theta)\cos\left(\phi - \frac{2\pi(m-1)}{M}\right)\right\}, \tag{4.16}$$

where $\omega = 2\pi f$ denotes angular frequency. The observations in frequency domain were written as

$$\mathrm{Y}(\omega) = \begin{bmatrix} Y_1(\omega) \\ Y_2(\omega) \\ Y_3(\omega) \\ \vdots \\ Y_M(\omega) \end{bmatrix} = Y(\omega)\begin{bmatrix} \exp\left\{i\frac{2\pi\, x_k}{\lambda}\sin(\theta)\cos(\phi)\right\} \\ \exp\left\{i\frac{2\pi x_k}{\lambda}\sin(\theta)\cos(\phi - \frac{2\pi}{M})\right\} \\ \exp\left\{i\frac{2\pi\, x_k}{\lambda}\sin(\theta)\cos(\phi - \frac{4\pi}{M})\right\} \\ \vdots \\ \exp\left\{i\frac{2\pi\, x_k}{\lambda}\sin(\theta)\cos(\phi - \frac{2\pi(M-1)}{M})\right\} \end{bmatrix}. \tag{4.17}$$

Since observations in frequency domain consists of the scalar and complex part, the array manifold vector was given by the complex part since the scalar part was constant

$$\boldsymbol{a}_{UHA} = \begin{bmatrix} \exp\left\{i\frac{2\pi\, x_k}{\lambda}\sin(\theta)\cos(\phi)\right\} \\ \exp\left\{i\frac{2\pi x_k}{\lambda}\sin(\theta)\cos(\phi - \frac{2\pi}{M})\right\} \\ \exp\left\{i\frac{2\pi\, x_k}{\lambda}\sin(\theta)\cos(\phi - \frac{4\pi}{M})\right\} \\ \vdots \\ \exp\left\{i\frac{2\pi\, x_k}{\lambda}\sin(\theta)\cos(\phi - \frac{2\pi(M-1)}{M})\right\} \end{bmatrix}. \tag{4.18}$$

4.1.1 Array Manifold Vector for Uniform Circular Array

The same procedures for deriving the array manifold vector for the uniform hexagonal were used here. The general position of the m^{th} for $m = 1,2,3\ldots$M was given by

$$\boldsymbol{P_{m=}}\left[Rcos\left(\frac{2\pi(m-1)}{M}\right), Rsin\left(\frac{2\pi(m-1)}{M}\right),\ 0\right]^T \tag{4.19}$$

Explicitly, using equation (4.19) and equation (4.14) in equation (4.13)

$$\tau_M = \frac{-1}{\lambda f}[\sin(\theta)\cos(\phi), \sin(\theta)\sin(\phi), \cos(\theta)] \begin{bmatrix} R\cos\left(\frac{2\pi(m-1)}{M}\right) \\ R\sin\left(\frac{2\pi(m-1)}{M}\right) \\ 0 \end{bmatrix} =$$

$$\frac{R\sin(\theta)}{\lambda f}\cos\left(\phi - \frac{2\pi(m-1)}{M}\right).$$

To convert the time domain signals into frequency domain, we took the Fourier transform of

y (t, p) from which we get the m^{th} component to be

$$Y_m(\omega) = \int_{-\infty}^{\infty} e^{-i\omega t}\, y(t - \tau_\ell)dt = Y(\omega)e^{-i\omega t}$$

$$= Y(\omega)exp\left\{\frac{i2\pi R}{\lambda}\sin(\theta)\cos\left(\phi - \frac{2\pi(m-1)}{M}\right)\right\}$$

The observations in frequency domain were written as

$$\mathrm{Y}(\omega) = \begin{bmatrix} Y_1(\omega) \\ Y_2(\omega) \\ Y_3(\omega) \\ \vdots \\ Y_M(\omega) \end{bmatrix} = Y(\omega) \begin{bmatrix} \exp\left\{i\frac{2\pi R}{\lambda}\sin(\theta)\cos(\phi)\right\} \\ \exp\left\{i\frac{2\pi R}{\lambda}\sin(\theta)\cos(\phi - \frac{2\pi}{M})\right\} \\ \exp\left\{i\frac{2\pi R}{\lambda}\sin(\theta)\cos(\phi - \frac{4\pi}{M})\right\} \\ \vdots \\ \exp\left\{i\frac{2\pi R}{\lambda}\sin(\theta)\cos(\phi - \frac{2\pi(M-1)}{M})\right\} \end{bmatrix} \quad (4.20)$$

Thus, the **array manifold vector** for a UCA was given by

$$\boldsymbol{a}_{UCA} = \begin{bmatrix} \exp\left\{i\frac{2\pi R}{\lambda}\sin(\theta)\cos(\phi)\right\} \\ \exp\left\{i\frac{2\pi R}{\lambda}\sin(\theta)\cos(\phi - \frac{2\pi}{M})\right\} \\ \exp\left\{i\frac{2\pi R}{\lambda}\sin(\theta)\cos(\phi - \frac{4\pi}{M})\right\} \\ \vdots \\ \exp\left\{i\frac{2\pi R}{\lambda}\sin(\theta)\cos(\phi - \frac{2\pi(M-1)}{M})\right\} \end{bmatrix}. \quad (4.21)$$

4.2 Derivation of the Cramér-Rao bound for the uniform hexagonal array

In this section a statistical data model was assumed, from the probability density function of the observed data vector the mean of the observed data was obtained, the mean of the observed data vector was used to derive the Fisher information matrix (FIM) of azimuth and polar angle. Finally, the inverse of the FIM gave the Cramér-Rao bound.

A signal model collected by all the sensors at time t was expressed as [32]

$$\mathbf{y}(\mathbf{m}) = \mathbf{a}\, \mathrm{s}(\mathrm{m}) + \mathbf{n}(\mathbf{m}) \qquad m = 1,2,3 \ldots\ldots\ldots\ldots M,$$

where s(m) is the signal released at time t, **a** is the array manifold vector that corresponded to the geometrical pattern under consideration and $\boldsymbol{n}$**(m)** is the additive noise. The observed data vector followed multivariate normal/Gaussian distribution. For multiple snapshots the data model vector was assumed to be given by [32]

$$\tilde{\boldsymbol{y}} = \boldsymbol{s} \otimes \boldsymbol{a}(\theta, \phi) + \tilde{\boldsymbol{n}} \tag{4.22}$$

Where

$$\tilde{\boldsymbol{y}} = [\boldsymbol{y}_1, \boldsymbol{y}_2, \cdots, \boldsymbol{y}_M]^T, \quad \boldsymbol{s} = s_1, s_2, \cdots s_M, \quad \boldsymbol{a} = a_1, a_2, \cdots, a_M \; and \; \tilde{\boldsymbol{n}} = [\boldsymbol{n}_1, \boldsymbol{n}_2, \cdots, \boldsymbol{n}_M]^T$$

The pdf of $\tilde{\boldsymbol{y}}$ was given by [2]

$$p(\tilde{\boldsymbol{y}}|\boldsymbol{\theta}) = \frac{\mathbf{1}}{\sqrt{|\mathbf{2}\boldsymbol{\pi}\tilde{\boldsymbol{\Gamma}}(\theta,\phi)|}} \exp\left\{-\frac{1}{2}[\tilde{\boldsymbol{y}} - \tilde{\boldsymbol{\mu}}(\theta,\phi)]^H \tilde{\boldsymbol{\Gamma}}(\theta,\phi)^{-1}[\tilde{\boldsymbol{y}} - \tilde{\boldsymbol{\mu}}(\theta,\phi)]\right\}, \tag{4.23}$$

where $\tilde{\boldsymbol{\mu}}(\theta,\phi) = E[\tilde{\boldsymbol{y}}] = \boldsymbol{s} \otimes \boldsymbol{a}(\theta,\phi)$, (4.24)

$$\tilde{\boldsymbol{\Gamma}}(\theta,\phi) = E\{[\tilde{\boldsymbol{y}} - \tilde{\boldsymbol{\mu}}(\theta,\phi)][\tilde{\boldsymbol{y}} - \tilde{\boldsymbol{\mu}}(\theta,\phi)]^H\} = \boldsymbol{\sigma}_{\boldsymbol{n}}^{\mathbf{2}} \boldsymbol{I}_{\{TM*TM\}}, \tag{4.25}$$

$E[\tilde{\boldsymbol{y}}]$ represents the statistical expectation of $\tilde{\boldsymbol{y}}$**,** $\boldsymbol{M}$ denotes the total number of sensors, $\boldsymbol{I}_{\{TM*TM\}}$ denotes an identity matrix of size TM, superscript H is the conjugate transpose and $\tilde{\boldsymbol{\Gamma}}$ is the covariance matrix of **y** and it's independent of θ and ϕ as shown in equation (4.25). Direction of arrival estimation aims to estimate the polar angle of arrival θ and the azimuth angle of arrival ϕ, based on the observations $\tilde{\boldsymbol{y}}$**.** We determined the FIM whose $(t,r)_{th}$ entry was given by equation (3.26).

Using equation (4.24) and equation (4.18) the partial derivative of $\boldsymbol{\mu}$ with respect to θ was given as

$$\frac{\partial \boldsymbol{\mu}}{\partial \theta} = \boldsymbol{s} \otimes \left\{ \begin{bmatrix} i\frac{2\pi x_k}{\lambda}\cos(\theta)\cos(\phi) \\ i\frac{2\pi x_k}{\lambda}\cos(\theta)\cos\left(\phi - \frac{2\pi}{M}\right) \\ \vdots \\ i\frac{2\pi x_k}{\lambda}\cos(\theta)\cos\left(\phi - \frac{2\pi(M-1)}{M}\right) \end{bmatrix} \odot \boldsymbol{a}(\theta,\phi) \right\}, \tag{4.26}$$

$$\frac{\partial \boldsymbol{\mu}}{\partial \phi} = \boldsymbol{s} \otimes \left\{ \begin{bmatrix} -i\frac{2\pi x_k}{\lambda}\sin(\theta)\cos(\phi) \\ -i\frac{2\pi x_k}{\lambda}\sin(\theta)\sin\left(\phi - \frac{2\pi}{M}\right) \\ \vdots \\ -i\frac{2\pi x_k}{\lambda}\sin(\theta)\sin\left(\phi - \frac{2\pi(M-1)}{M}\right) \end{bmatrix} \odot \boldsymbol{a}(\theta,\phi) \right\}, \tag{4.27}$$

Where $\odot$ and $\otimes$ denotes Hadamard product and Kronecker product respectively.

Using equation (4.26) -(4.27) the elements of the Fisher information matrix were obtained as follows

$$F_{\theta,\theta} = 2Re\left\{ \left[\frac{\partial \boldsymbol{\mu}}{\partial \theta}\right]^H [\Gamma]^{-1} \left[\frac{\partial \boldsymbol{\mu}}{\partial \theta}\right] \right\} = \frac{2}{\sigma_n^2}\left[\frac{\partial \boldsymbol{\mu}}{\partial \theta}\right]^H \left[\frac{\partial \boldsymbol{\mu}}{\partial \theta}\right] =$$

$$= 2\left[\frac{2\pi x_k \cos(\theta)}{\lambda \sigma_n}\right]^2 s^H s \left[\cos^2(\phi) + \cos^2\left(\phi - \frac{2\pi}{M}\right) + \cdots + \cos^2\left(\phi - \frac{2\pi(M-1)}{M}\right)\right]$$

$$= 2\left[\frac{2\pi x_k \cos(\theta)}{\lambda \sigma_n}\right]^2 \sigma_n^2 \underbrace{[1 + 1 + \cdots + 1]}_{T\ times} \underbrace{\sum_{m=1}^{M} \cos^2\left(\phi - \frac{2\pi(m-1)}{M}\right)}_{\frac{M}{2}}$$

where

$$s^H s = \begin{bmatrix} \sigma_s e^{-\{2\pi f+\varphi\}} \\ \sigma_s e^{-\{4\pi f+\varphi\}} \\ \vdots \\ \sigma_s e^{-\{2\pi fT+\varphi\}} \end{bmatrix}^H \begin{bmatrix} \sigma_s e^{-\{2\pi f+\varphi\}} \\ \sigma_s e^{-\{4\pi f+\varphi\}} \\ \vdots \\ \sigma_s e^{-\{2\pi fT+\varphi\}} \end{bmatrix} = \sigma_s^2 \begin{bmatrix} 1 \\ 1 \\ \vdots \\ 1 \end{bmatrix}$$

$$\sum_{m=1}^{M} \cos^2\left(\phi - \frac{2\pi(m-1)}{M}\right) = \sum_{m=0}^{M-1} \cos^2\left(\phi - \frac{2\pi m}{M}\right)$$

$$= \sum_{m=0}^{M-1} \left[\cos\left(\frac{2\pi m}{M}\right)\cos(\phi) + \sin\left(\frac{2\pi m}{M}\right)\sin(\phi)\right]$$

$$= \sum_{m=0}^{M-1} \left[\cos^2\left(\frac{2\pi m}{M}\right)\cos^2(\phi) + \sin^2\left(\frac{2\pi m}{M}\right)\sin^2(\phi) + 2\cos\left(\frac{2\pi m}{M}\right)\cos(\phi)\sin\left(\frac{2\pi m}{M}\right)\sin(\phi)\right]$$

$$= \cos^2(\phi)\sum_{m=0}^{M-1} \cos^2\left(\frac{2\pi m}{M}\right) + \sin^2(\phi)\sum_{m=0}^{M-1} \sin^2\left(\frac{2\pi m}{M}\right) + \frac{\sin(2\phi)}{2}\sum_{m=0}^{M-1} \sin\left(\frac{4\pi m}{M}\right)$$

$$\sum_{m=0}^{M-1} \cos^2\left(\frac{2\pi m}{M}\right) = 1 + \cos^2\left(\frac{2\pi}{M}\right) + \cos^2\left(\frac{4\pi}{M}\right) + \cdots + \cos^2\left(\frac{2\pi(m-1)}{M}\right)$$

$$= 1 + \cos^2(2\phi) + \cos^2(4\phi) + \cdots + \cos^2(2\phi(m-1))$$

$$= 1 + \frac{1+\cos^2(2\phi)}{2} + \frac{1+\cos^2(4\phi)}{2} + \cdots + \frac{1+\cos^2(2\phi)(m-1)}{2}$$

$$= \frac{1}{2}[2 + 1 + \cos^2(2\phi) + 1 + \cos^2(4\phi) + \cdots + 1 + \cos^2(2\phi)(m-1)]$$

$$= \frac{1}{2}[M + 1 + \cos^2(2\phi) + \cos^2(4\phi) + \cdots + \cos^2(2\phi)(m-1)]$$

$$= \frac{1}{2}\left[M + 1 + \frac{\sin\left(4\pi+\frac{2\pi}{M}\right)-\sin\left(\frac{2\pi}{M}\right)}{2\sin\left(\frac{2\pi}{M}\right)} - \cos(4\pi)\right] = \frac{M}{2}$$

$$\sum_{m=0}^{M-1} \sin^2\left(\frac{2\pi m}{M}\right) = \sin^2\left(\frac{2\pi}{M}\right) + \sin^2\left(\frac{4\pi}{M}\right) + \cdots + \sin^2\left(\frac{2\pi(m-1)}{M}\right)$$

$$= \sin^2(2\phi) + \sin^2(4\phi) + \cdots + \sin^2(2\phi(m-1))$$

$$= \frac{1-\cos^2(\phi)}{2} + \frac{1-\cos^2(4\phi)}{2} + \cdots + \frac{1-\cos^2(2\phi)(m-1)}{2}$$

$$= \frac{1}{2}[1 - \cos^2(2\phi) + 1 - \cos^2(4\phi) + \cdots + 1 - \cos^2(2\phi)(m-1)]$$

$$= \frac{1}{2}\left[M - \left[1 + \frac{\sin\left(4\pi+\frac{2\pi}{M}\right)-\sin\left(\frac{2\pi}{M}\right)}{2\sin\left(\frac{2\pi}{M}\right)} - \cos(4\pi)\right]\right] = \frac{M}{2},$$

$$\sum_{m=0}^{M-1} \; sin\left(\frac{4\pi m}{M}\right) = \sin\left(\frac{4\pi}{M}\right) + \sin\left(\frac{8\pi}{M}\right) + \cdots + \sin\left(\frac{4\pi(m-1)}{M}\right)$$

$$= \sin(r) + \sin(2r) + \cdots + \sin(r(m-1))$$

$$= \frac{\cos\left(\frac{2\pi}{M}\right)-\cos\left(4\pi+\frac{2\pi}{M}\right)}{2\sin\left(\frac{2\pi}{M}\right)} - \sin(4\pi)$$

$$= \frac{\cos\left(\frac{2\pi}{M}\right)-\cos\left(\frac{2\pi}{M}\right)}{2\sin\left(\frac{2\pi}{M}\right)} - \sin(4\pi) = 0$$

$$\sum_{m=1}^{M} \cos^2\left(\phi - \frac{2\pi(m-1)}{M}\right) = \cos^2(\phi) \underbrace{\sum_{m=0}^{M-1} \; \cos^2\left(\frac{2\pi m}{M}\right)}_{=\frac{M}{2}} +$$

$$\sin^2(\phi) \underbrace{\sum_{m=0}^{M-1} \; \sin^2\left(\frac{2\pi m}{M}\right)}_{=\frac{M}{2}} + \frac{\sin(2\phi)}{2} \underbrace{\sum_{m=0}^{M-1} \; sin\left(\frac{4\pi m}{M}\right)}_{0}$$

$$F_{\theta,\theta} = 4\pi^2 MT\left(\frac{x_k}{\lambda}\right)^2\left(\frac{\sigma_s}{\sigma_n}\right)^2 \cos^2(\theta). \tag{4.28}$$

$$F_{\phi,\phi} = 2Re\left\{\left[\frac{\partial \boldsymbol{\mu}}{\partial \phi}\right]^H [\Gamma]^{-1} \left[\frac{\partial \boldsymbol{\mu}}{\partial \phi}\right]\right\} = \frac{2}{\sigma_n^2}\left[\frac{\partial \boldsymbol{\mu}}{\partial \phi}\right]^H \left[\frac{\partial \boldsymbol{\mu}}{\partial \phi}\right] =$$

$$= \; 2\left[\frac{2\pi x_k \cos(\theta)}{\lambda\sigma_n}\right]^2 s^H s\left[\cos^2(\phi) + \cos^2\left(\phi - \frac{2\pi}{M}\right) + \cdots + \cos^2\left(\phi - \frac{2\pi(M-1)}{M}\right)\right]$$

$$= 2\left[\frac{2\pi x_k \sin(\theta)}{\lambda\sigma_n}\right]^2 \sigma_n^2 \underbrace{[1 + 1 + \cdots + 1]}_{T\ times} \underbrace{\sum_{m=1}^{M} \sin^2\left(\phi - \frac{2\pi(m-1)}{M}\right)}_{\frac{M}{2}}$$

$$\sum_{m=1}^{M} \sin^2\left(\phi - \frac{2\pi(m-1)}{M}\right) = \sum_{m=0}^{M-1} \sin^2\left(\phi - \frac{2\pi m}{M}\right)$$

$$= \sum_{m=0}^{M-1} \left[\sin\left(\frac{2\pi m}{M}\right)\cos(\phi) - \cos\left(\frac{2\pi m}{M}\right)\sin(\phi)\right]^2$$

$$= \sum_{m=0}^{M-1} \left[\sin^2\left(\frac{2\pi m}{M}\right)\cos^2(\phi) + \cos^2\left(\frac{2\pi m}{M}\right)\sin^2(\phi) - 2\cos\left(\frac{2\pi m}{M}\right)\cos(\phi)\sin\left(\frac{2\pi m}{M}\right)\cos(\phi)\right]$$

$$= \cos^2(\phi)\underbrace{\sum_{m=0}^{M-1} \sin^2\left(\frac{2\pi m}{M}\right)}_{=\frac{M}{2}} + \sin^2(\phi)\underbrace{\sum_{m=0}^{M-1} \cos^2\left(\frac{2\pi m}{M}\right)}_{=\frac{M}{2}} - \frac{\sin(2\phi)}{2}\underbrace{\sum_{m=0}^{M-1} sin\left(\frac{4\pi m}{M}\right)}_{=0} = \frac{M}{2}$$

$$F_{\phi,\phi} = 4\pi^2 MT\left(\frac{x_k}{\lambda}\right)^2\left(\frac{\sigma_s}{\sigma_n}\right)^2 \sin^2(\theta). \tag{4.29}$$

$$F_{\theta,\phi} = F_{\phi,\theta} = 2Re\left\{\left[\frac{\partial \boldsymbol{\mu}}{\partial\theta}\right]^H [\Gamma]^{-1}\left[\frac{\partial \boldsymbol{\mu}}{\partial\phi}\right]\right\} \tag{4.30}$$

$$= \frac{4\pi^2 x_k^2 \sigma_n^2 \sin(\theta)\cos(\theta)}{\lambda^2\sigma_n^2}\underbrace{[1+1+\cdots+1]}_{T\ times}\underbrace{\sum_{m=1}^{M} sin\left(\phi - \frac{2\pi(m-1)}{M}\right)cos\left(\phi - \frac{2\pi(m-1)}{M}\right)}_{=0} = 0.$$

The CRB were obtained as shown below

$$\begin{bmatrix} [\mathrm{CRB}(\theta)]_{1,1} & 0 \\ 0 & [\mathrm{CRB}(\phi)]_{2,2} \end{bmatrix} = \begin{bmatrix} F_{\theta,\theta} & F_{\theta,\phi} \\ F_{\phi,\theta} & F_{\phi,\phi} \end{bmatrix}^{-1} = \begin{bmatrix} \frac{1}{F_{\theta,\theta}} & 0 \\ 0 & \frac{1}{F_{\phi,\phi}} \end{bmatrix}, \tag{4.31}$$

From equation (4.28) to (4.31)

$$CRB_{UHA}(\theta) = \frac{1}{F_{\theta,\theta}} = \frac{1}{4\pi^2}\frac{1}{MT}\left(\frac{\lambda}{x_k}\right)^2\left(\frac{\sigma_n}{\sigma_s}\right)^2 \sec^2(\theta), \tag{4.32}$$

$$CRB_{UHA}(\phi) = \frac{1}{F_{\phi,\phi}} = \frac{1}{4\pi^2}\frac{1}{MT}\left(\frac{\lambda}{x_k}\right)^2\left(\frac{\sigma_n}{\sigma_s}\right)^2 \csc^2(\theta), \tag{4.33}$$

where T denotes the total number of time signals and M is the total number of the sensors.

4.2.1 Cramér-Rao bound for the uniform circular array

Using equation (4.24) and equation (4.21)

$$\frac{\partial \boldsymbol{\mu}}{\partial \theta} = \boldsymbol{s} \otimes \left\{ \begin{bmatrix} i\frac{2\pi R}{\lambda}\cos(\theta)\cos(\phi) \\ i\frac{2\pi R}{\lambda}\cos(\theta)\cos\left(\phi - \frac{2\pi}{M}\right) \\ \vdots \\ i\frac{2\pi R}{\lambda}\cos(\theta)\cos\left(\phi - \frac{2\pi(M-1)}{M}\right) \end{bmatrix} \odot \boldsymbol{a}(\theta,\phi) \right\}, \tag{4.34}$$

$$\frac{\partial \boldsymbol{\mu}}{\partial \phi} = \boldsymbol{s} \otimes \left\{ \begin{bmatrix} -i\frac{2\pi R}{\lambda}\sin(\theta)\cos(\phi) \\ -i\frac{2\pi R}{\lambda}\sin(\theta)\sin\left(\phi - \frac{2\pi}{M}\right) \\ \vdots \\ -i\frac{2\pi R}{\lambda}\sin(\theta)\sin\left(\phi - \frac{2\pi(M-1)}{M}\right) \end{bmatrix} \odot \boldsymbol{a}(\theta,\phi) \right\}, \tag{4.35}$$

Where $\odot$ and $\otimes$ denotes Hadamard product and Kronecker product respectively.

Using equation (4.26) and equation (4.35) -(4.36) the elements of the Fisher information matrix were obtained as follows

$$F_{\theta,\theta} = 2Re\left\{\left[\frac{\partial \boldsymbol{\mu}}{\partial \theta}\right]^H [\Gamma]^{-1}\left[\frac{\partial \boldsymbol{\mu}}{\partial \theta}\right]\right\} = \frac{2}{\sigma_n^2}\left[\frac{\partial \boldsymbol{\mu}}{\partial \theta}\right]^H\left[\frac{\partial \boldsymbol{\mu}}{\partial \theta}\right] = \tag{4.36}$$

$$= 2\left[\frac{2\pi R\cos(\theta)}{\lambda\sigma_n}\right]^2 s^H s\left[\cos^2(\phi) + \cos^2\left(\phi - \frac{2\pi}{M}\right) + \cdots + \cos^2\left(\phi - \frac{2\pi(M-1)}{M}\right)\right]$$

$$= 2\left[\frac{2\pi R\cos(\theta)}{\lambda\sigma_n}\right]^2 \sigma_n^2 \underbrace{[1+1+\cdots+1]}_{T\ times} \underbrace{\sum_{m=1}^{M}\cos^2\left(\phi-\frac{2\pi(m-1)}{M}\right)}_{\frac{M}{2}}$$

$$= 4\pi^2 MT\left(\frac{R}{\lambda}\right)^2\left(\frac{\sigma_s}{\sigma_n}\right)^2\cos^2(\theta)$$

$$F_{\phi,\phi} = 2Re\left\{\left[\frac{\partial\boldsymbol{\mu}}{\partial\phi}\right]^H[\Gamma]^{-1}\left[\frac{\partial\boldsymbol{\mu}}{\partial\phi}\right]\right\} = \frac{2}{\sigma_n^2}\left[\frac{\partial\boldsymbol{\mu}}{\partial\phi}\right]^H\left[\frac{\partial\boldsymbol{\mu}}{\partial\phi}\right] = \tag{4.37}$$

$$= 2\left[\frac{2\pi R\cos(\theta)}{\lambda\sigma_n}\right]^2 s^H s\left[\cos^2(\phi)+\cos^2\left(\phi-\frac{2\pi}{M}\right)+\cdots+\cos^2\left(\phi-\frac{2\pi(M-1)}{M}\right)\right]$$

$$= 2\left[\frac{2\pi R\sin(\theta)}{\lambda\sigma_n}\right]^2 \sigma_n^2 \underbrace{[1+1+\cdots+1]}_{T\ times} \underbrace{\sum_{m=1}^{M}\sin^2\left(\phi-\frac{2\pi(m-1)}{M}\right)}_{\frac{M}{2}}$$

$$= 4\pi^2 MT\left(\frac{R}{\lambda}\right)^2\left(\frac{\sigma_s}{\sigma_n}\right)^2\sin^2(\theta)$$

$$F_{\theta,\phi} = F_{\phi,\theta} = 2Re\left\{\left[\frac{\partial\boldsymbol{\mu}}{\partial\theta}\right]^H[\Gamma]^{-1}\left[\frac{\partial\boldsymbol{\mu}}{\partial\phi}\right]\right\} \tag{4.38}$$

$$= \frac{4\pi^2R^2\sigma_n^2\sin(\theta)\cos(\theta)}{\lambda^2\sigma_n^2} \underbrace{[1+1+\cdots+1]}_{T\ times} \underbrace{\sum_{m=1}^{M} sin\left(\phi-\frac{2\pi(m-1)}{M}\right)cos\left(\phi-\frac{2\pi(m-1)}{M}\right)}_{=0} = 0.$$

From equation (4.31) and equation (4.36) -(4.38)

$$CRB_{UCA}(\theta) = \frac{1}{F_{\theta,\theta}} = \frac{1}{4\pi^2}\frac{1}{MT}\left(\frac{\lambda}{R}\right)^2\left(\frac{\sigma_n}{\sigma_s}\right)^2\sec^2(\theta), \tag{4.39}$$

$$CRB_{UCA}(\phi) = \frac{1}{F_{\phi,\phi}} = \frac{1}{4\pi^2}\frac{1}{MT}\left(\frac{\lambda}{R}\right)^2\left(\frac{\sigma_n}{\sigma_s}\right)^2\csc^2(\theta). \tag{4.40}$$

4.3 Comparison of the Cramér-Rao bound of uniform hexagonal array and that of uniform circular array

The derived Cramér-Rao bound for the uniform hexagonal is compared with the Cramér-Rao bound for the uniform circular array using the ratio in this section. The ratio $\frac{CRB_{UHA}}{CRB_{UCA}}$ is analyzed into three possible scenarios, the first case is when the ratio $\frac{CRB_{UHA}}{CRB_{UCA}}$ is less than one, the second case is when the ratio $\frac{CRB_{UHA}}{CRB_{UCA}}$ is greater than one and finally, when the ratio $\frac{CRB_{UHA}}{CRB_{UCA}}$ is equal to one. These results are validated by graphical representation.

From equation (4.32) -(4.33) and equation (4.39) -(4.40) the ratio of Cramér-Rao bound of uniform hexagonal array to that of uniform circular array is;

$$\frac{CRB_{UHA}(\theta)}{CRB_{UCA}(\theta)} = \frac{CRB_{UHA}(\phi)}{CRB_{UCA}(\phi)} = \left(\frac{2}{\sqrt{3+\left[\frac{2k-1}{n-1}\right]^2}}\right)^2 =: \frac{CRB_{UHA}}{CRB_{UCA}} \tag{4.41}$$

Where CRB_{UHA} and CRB_{UCA} denote CRBs of UHA and UCA respectively.

We considered all possible scenarios of equation (4.41) as analyzed in the following cases.

When the ratio $\frac{CRB_{UHA}}{CRB_{UCA}}$ is greater than one

Case 1: $$\left(\frac{2}{\sqrt{3+\left[\frac{2k-1}{n-1}\right]^2}}\right)^2 > 1 \Leftrightarrow \sqrt{3+\left[\frac{2k-1}{n-1}\right]^2} < 2 \Leftrightarrow k < \frac{n}{2}. \tag{4.42}$$

Equation (4.42) for

$$\begin{matrix} n = 4; k = 1; M = 18 \\ n = 6; k = 1, 2; M = 30 \\ \vdots \end{matrix}.$$

Example of case 1 consider condition $n = 6; k = 1, 2; M = 30$

$$CRB_{UHA}(\theta) = \frac{1}{4\pi^2}\frac{1}{30T}\left(\frac{1.14707\lambda}{R}\right)^2\left(\frac{\sigma_n}{\sigma_s}\right)^2 \sec^2(\theta) \tag{4.43}$$

$$CRB_{UCA}(\theta) = \frac{1}{4\pi^2}\frac{1}{30T}\left(\frac{\lambda}{R}\right)^2\left(\frac{\sigma_n}{\sigma_s}\right)^2 \sec^2(\theta) \tag{4.44}$$

When the $\frac{CRB_{UHA}}{CRB_{UCA}}$ is less than one

Case 2: $$\left(\frac{2}{\sqrt{3+\left[\frac{2k-1}{n-1}\right]^2}}\right)^2 < 1 \Leftrightarrow \sqrt{3+\left[\frac{2k-1}{n-1}\right]^2} > 2 \Leftrightarrow k > \frac{n}{2} \quad (4.45)$$

This case is not a possible scenario since the general distance derived in equation (4.11) holds for k not exceeding $\frac{n}{2}$ Thus it is established that under no circumstance will CRB_{UHA} be lower than CRB_{UCA}.

When the ratio $\frac{CRB_{UHA}}{CRB_{UCA}}$ is equal to one

Case 3: $$\left(\frac{2}{\sqrt{3+\left[\frac{2k-1}{n-1}\right]^2}}\right)^2 = 1 \Leftrightarrow \sqrt{3+\left[\frac{2k-1}{n-1}\right]^2} = 2 \Leftrightarrow k = \frac{n}{2} \quad (4.46)$$

Equation (5.15) holds $\begin{matrix} n=2; k=1; M=6 \\ n=4; k=2; M=18 \\ \vdots \end{matrix}$.

Example of case 3 consider condition $n = 6; k = 1, 2; M = 30$

$$CRB_{UHA}(\theta) = \frac{1}{4\pi^2}\frac{1}{6T}\left(\frac{\lambda}{R}\right)^2\left(\frac{\sigma_n}{\sigma_s}\right)^2 \sec^2(\theta), \quad (4.47)$$

$$CRB_{UCA}(\theta) = \frac{1}{4\pi^2}\frac{1}{6T}\left(\frac{\lambda}{R}\right)^2\left(\frac{\sigma_n}{\sigma_s}\right)^2 \sec^2(\theta). \quad (4.48)$$

In the above, $n = 2, 4, 6 \ldots N$ denotes the total number of the sensors on one of the equilateral triangles of the uniform hexagonal array and M is the total number of the sensors.

4.3.1 Graphical Representation

In this sub-section, the graphical analysis is provided to investigate the performance analysis of uniform hexagonal array and uniform circular in direction of arrival estimation accuracy.

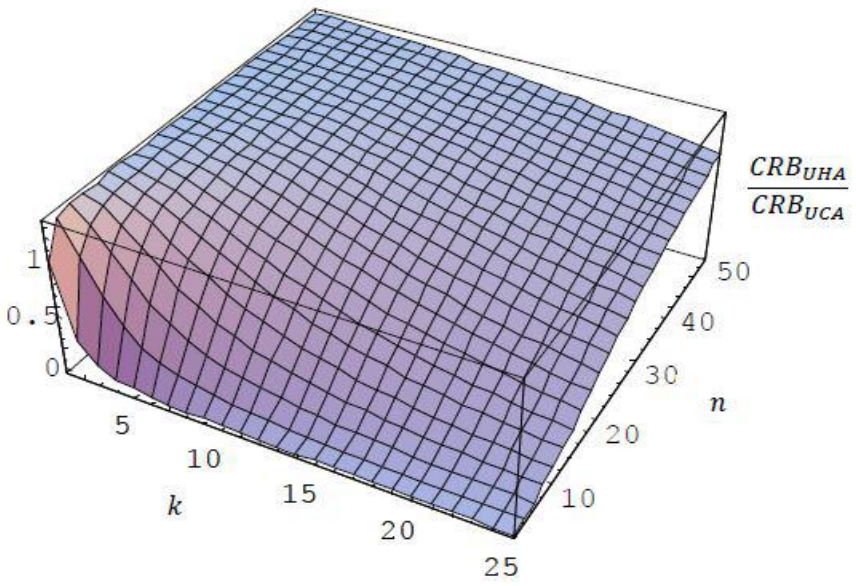

Fig. 4. 1: The figure shows how the ratio $\frac{CRB_{UHA}}{CRB_{UCA}}$ changes as n and k changes

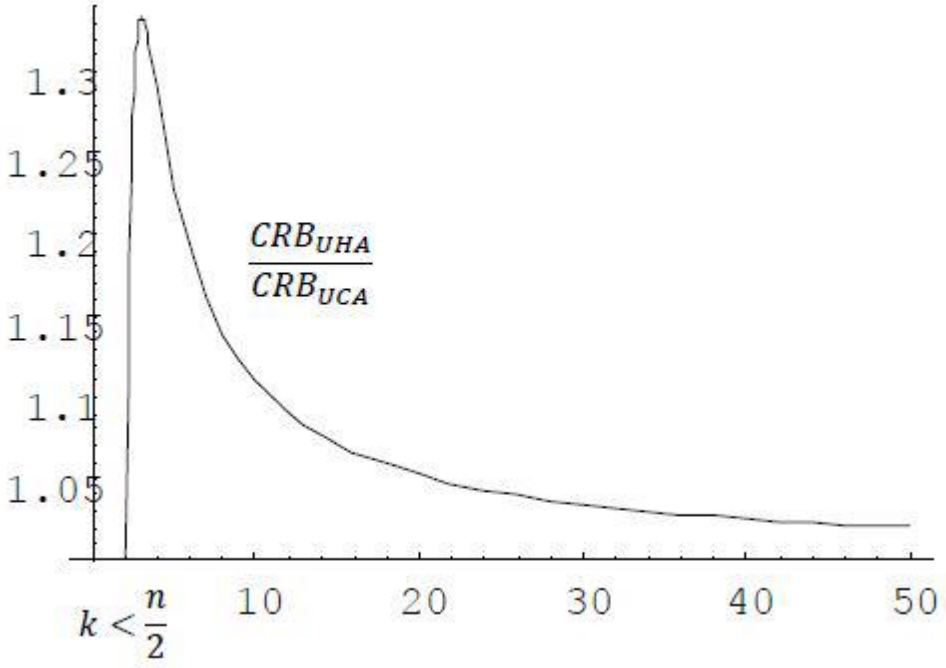

Fig. 4. 2: The figure shows how the ratio $\frac{CRB_{UHA}}{CRB_{UCA}}$ changes as $k < \frac{n}{2}$ varies.

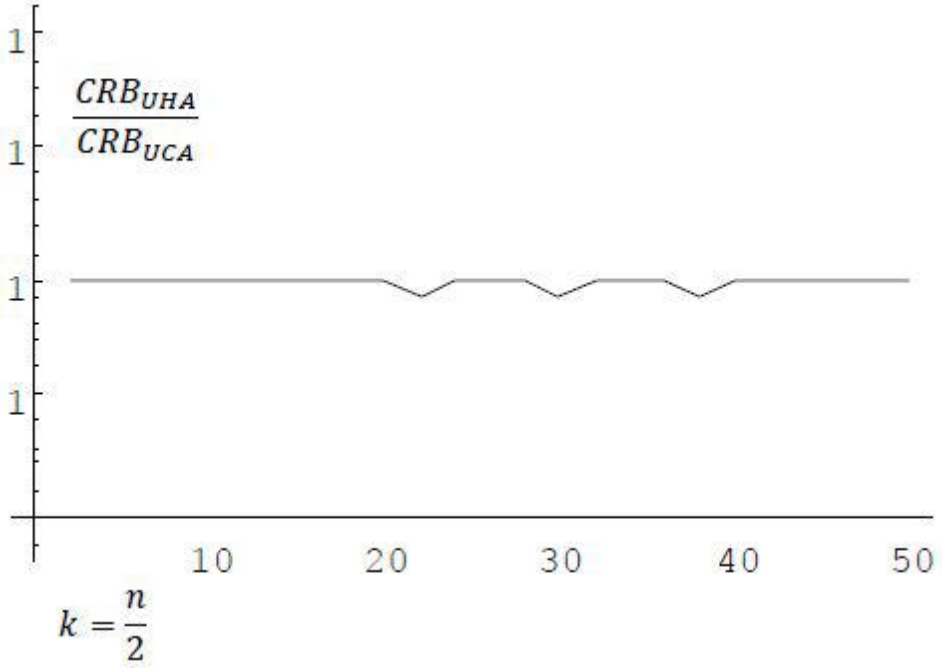

Fig. 4. 3: The figure shows how the ratio $\frac{CRB_{UHA}}{CRB_{UCA}}$ changes as $k = \frac{n}{2}$ varies.

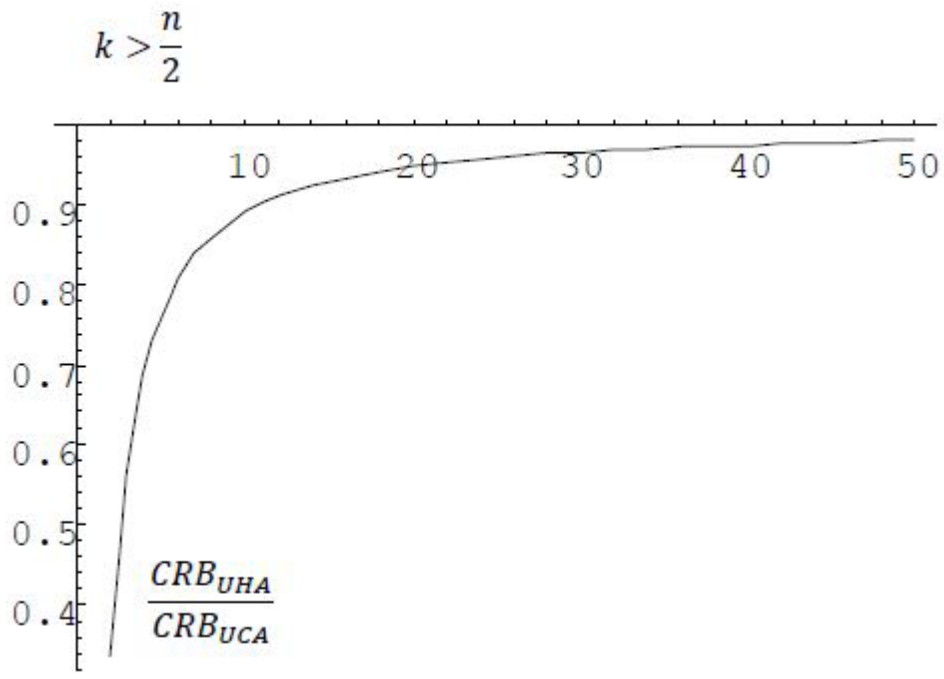

Fig. 4. 4: The figure shows how the ratio $\frac{CRB_{UHA}}{CRB_{UCA}}$ changes as $k > \frac{n}{2}$ varies.

Fig. 4.1 to Fig. 4. 4 represent the graphical analysis of the ratio developed from the analytical results. Figure. 4. 1 shows that, the increase in n and k results into an increase in the ratio $\frac{CRB_{UHA}}{CRB_{UCA}}$. Fig. 4.2 indicates that when $k < \frac{n}{2}$ increases, it results in a decrease in the ratio, implying that the uniform circular array performs better than uniform hexagonal array in this case. Since, the CRB of the UCA is a smaller as compared to that of UHA when the number of sensors is increased. When $k = 2$, the ratio is equal to one but at point $20;\ 30;\ 40$ there is some depression this is as a result of bifurcation as n crosses some values. The values of the ratio at those points still equals to one as shown in Fig. 4. 3, implying that UHA and UCA have the same performance since their CRBs are equal as the number of sensors is increased. When the ratio is equal to one either UCA or UHA can be used in direction of arrival estimation. Finally, the case when $k > \frac{n}{2}$ is not a possible scenario case for the UHA since the ratio is converging to zero, as indicated in Fig. 4.4, but CRB for the UCA decreases with increase in the number of sensors, therefore, it performs better than UHA in this case. Thus, UCA is more superior than UHA in direction of arrival estimation.

Normalized Sensitivity Analysis

Sensitive analysis is an algorithm that is used to determine how self-reliant variable values will influence a particular reliant variable under certain presumption. It helps to examine how sensitive the output is, by the changes in one input while holding the other input constant. Let

$$\frac{CRB_{UHA}}{CRB_{UCA}} = \frac{4}{3+\left[\frac{2k-1}{n-1}\right]^2} = \frac{4(n-1)^2}{3(n-1)^2+(2k-1)^2} \tag{4.49}$$

The normalized sensitivity analysis of a parameter $\boldsymbol{\omega}$ in $f(\omega)$ is given by

$S = \frac{\partial f}{\partial \omega}\frac{\omega}{f}$.

We can normalize about some point n and k:

$$S_n^1 = \frac{\partial R}{\partial n}\frac{n}{R} = \frac{2(1-2k)^2 n}{(n-1)\{(4+4(k-1))\}k+3(n-2)n}. \tag{4.50}$$

$$S_k^1 = \frac{\partial R}{\partial k}\frac{k}{R} = -\frac{4(2k-1)}{(2k-1)^2+3(n-1)^2}. \tag{4.51}$$

The normalized sensitivity of equation (4.50) shows that the ratio increases with increase in n,
since S_n^1 is always positive for $n \geq 2$ and $k \geq 1$. While equation (4.51) shows that the ratio decreases in k since is always negative for $n \geq 2$ and $k \geq 1$.

4.4 Discussion

From the above results the array manifold vector and CRB for the uniform hexagonal array have been derived. It was observed that when the number of sensors increases the CRB for the UHA reduces, thus for the direction of arrival estimation the UHA can be employed when the number of sensors is increased. From the comparison of the CRB for UHA and that of UCA it was observed that in the first case the CRB_{UHA} were higher as compared to CRB_{UCA}, implying that UCA has better performance as compared to UHA for the accuracy of DOA estimation.

In this case the uniform circular array still had better estimation accuracy for DOA estimation. In the second case when the ratio was equal to one UHA and UCA had equal CRB, thus having the same performance for the direction-finding estimation. In the final case either UHA or UCA can be used for direction finding. In the third case when the ratio was greater than one, it was observed that this case was not a possible scenario since the general distance obtained in equation (4.11) holds for k not exceeding $\frac{n}{2}$. Thus, it was established that under no circumstance will CRB_{UHA} be lower than CRB_{UCA}.

CHAPTER FIVE

CONCLUSION AND RECOMMENDATIONS

5.1 Conclusion

In this section, a summary of the results on the array manifold vector, Cramér-Rao bound and comparison of the Cramér-Rao bound for UHA and UCA is given.

This project suggested a new approach to estimate the accuracy of DOA estimation with Cramér-Rao bound through the uniform hexagonal array. This performance is accomplished first by deriving the array manifold vector for the uniform hexagonal array. The second step applies the array manifold vector obtained from the first step, to the mean of the observed data vector in order to derive the Cramér-Rao bound for UHA. Finally, the accuracy of DOA is achieved by comparing the derived Cramér-Rao bound for UHA with the Cramér-Rao bound for UCA. The main contents of this research work are summarized as follows; Cramér-Rao bound for uniform hexagonal array decreases with an increase in the number of sensors, therefore, UHA can be used in direction of arrival estimation when the number of sensors increases. The comparison between hexagonal and circular arrays shows that hexagonal array geometry gives slightly higher Cram´er-Rao bound by approximately

$$\frac{CRB_{UHA}(\theta)}{CRB_{UCA}(\theta)} = \frac{CRB_{UHA}(\phi)}{CRB_{UCA}(\phi)} = \frac{2}{\sqrt{3+\left[\frac{2k-1}{n-1}\right]^2}} \tag{5.11}$$

with respect to circular array. The CRB for the UHA is higher as compared to the CRB of UCA.

Therefore, uniform circular array has better estimation accuracy for the DOA estimation as compared to the uniform hexagonal array. This study contributes to the improvement of wireless communication, radar, military surveillance and speech among others. Therefore, wireless network designers, radar designers, and military surveillance designers can employ this method and geometry to improve their reliabilities when the number of sensors increases.

5.2 Recommendation for future work

This work was proposed to determine the accuracy of direction of arrival estimation using uniform hexagonal array employing CRB. In this section, we address other geometries and methods that can be investigated in future studies. Although the direction of arrival estimation theory and other technologies in an array sensor setting have become well established some further investigations can be conducted.

Current research efforts have paid more attention to the polygon with equal inter-sensor spacing. The non-uniform polygons for the direction of arrival estimation need to be addressed. One dimension and two-dimension uniform arrays are in place, but little research on three-dimension arrays has been done. Three-dimension investigation is more in accordance with real-time environments where three angles of arrival are needed. More researchers are concerned with the direction of arrival without considering the factors that affect DOA estimation such as, electromagnetic interference, channel band with inconsistency, and mutual coupling. The mutual coupling between the sensors distorts the array output signal and degrades the performance of DOA estimation. Its coefficient can be updated in an adaptive manner to guarantee convergence. The adaptation of all other geometries using CRB can be investigated in the same way and their performance can be compared. Moreover, trying to reproduce the results with a MATLAB will be an interesting step. Finally, the performance of the geometries proposed in this research can be analyzed more profoundly by evaluating the effects of other parameters such as signal-to-noise ratio, different inter-sensor spacing and the number of snapshots.

REFERENCES

[1] N. A. Dheringe and B. N. Bansode, "Performance Evaluation and Analysis of Direction of Arrival Estimation Using MUSIC, TLS ESPRIT and Pro ESPRIT Algorithms", *International Journal of Advanced Research in Electrical, Electronics and Instrumentation Engineering*, vol. 4(6), pp. 4948-4958, 2015.

[2] S. M. Kay, "Fundamental of Statistical Signal Processing: Estimation Theory", *Upper Saddle River, New Jersey: Prentice Hall*, 1993.

[3] M. A. Ihedrane and B. R. Seddik, "Direction of arrival estimation using MUSIC, ESPRIT and maximum-likelihood algorithms for antenna arrays," *Walailak Journal of Science and Technology (WJST)*, vol. 13, no. 6, pp. 491502, 2015.

[4] E. Aboutanios, A. Hassanien, A. El-Keyi, Y. Nasser, and S. A. Vorobyov, "Advances in DOA Estimation and Source Localization", *International Journal of Antennas and Propagation,* 2017.

[5] Y. E. G. Guzman, "Compressed Sensing Algorithms for Direction of Arrival (DoA) Estimation", 2017.

[6] R. A. Mendez, J. F. Silva, R. Orostica, and R. Lobos, "Analysis of the Cram´er-Rao bound in the joint estimation of astrometry and photometry," *Publication of Astronomical Society of the Pacific 2016*, vol. 942, pp. 798, 2014.

[7] Z. Xiaofei, L. Jianfeng, and X. Lingyun, "Novel two-dimensional DOA estimation with L-shaped array," *EURASIP Journal on Advances in Signal Processing,* pp. 1-7, 2011.

[8] J. Chao, E. S. Ward, and R. J. Ober, "Fisher information theory for parameter estimation in single molecule microscopy," vol. 33, no. 7, pp. B36-B57, 2016.

[9] G. P. Gera and B. Mulgrew, "Antenna array Cramer-Rao bound design by element relocation*," In 2009 17th European Signal Processing Conference*, pp. 1141-1145, 2009.

[10] M. Li, Y. Lu and B. He, "Array signal processing for maximum likelihood direction-of-arrival estimation," *Journal of Electrical and Electronic Systems*, vol. 3, pp. 117, 2013.

[11] J. T. Kim, S. T. Kim, and K. W. Lee, "Ambiguity analysis method for the calibrated array manifold," 2013.

[12] Z. Tian and H. L. Van Trees, "DoA estimation with hexagonal arrays*," In Proceeding of the 1998 IEEE International Conference on Acoustic, Speech and Signal processing, ICASSP'98*, vol. 4, pp. 2053-2056, 1998.

[13] L. Gupta and R. P. Singh, "Direction of arrival estimation," *International Journal of Advanced Engineering Technology*, 2010.

[14] B. Sun, "MUSIC based on uniform circular array and its direction-finding efficiency," *Inte. J. Sign. Proc. Syst,* vol. 1, pp. 273-277, 2013.

[15] T. Li and A. Nehorai, "Maximum likelihood direction finding in spatially colored noise fields using sparse sensors arrays," IEEE *Transaction on Signal processing,* vol. 59(3), ppp.1048-1062, 2011.

[16] E. Kwizera, E. Mwangi, and D. B. Konditi, "Performance Evaluation of Direction of Arrival Estimation using Uniform and Non-uniform Linear Arrays," *Journal of sustainable research in engineering,* vol. 3, no. 2, pp. 29-36, 2017.

[17] A. Vesa, "Direction-of-Arrival Estimation in case of Uniform Sensor Array using the MUSIC Algorithm," *Transactions on electronics and communication,* vol. 56, pp. 40.

[18] H. Gazzah, J. P. Delmas, and S. M. Larsys, "Direction-finding arrays of directional sensors for randomly located sources," *IEEE Transactions on Aerospace and Electronic Systems,* vol. 52, pp. 1995-2003, 2016.

[19] B. J. Jackson, S. Rajan, B. J. Liao and S. Wang, "Direction of arrival estimation using directive antennas in uniform circular arrays," *IEEE Transactions on Antennas and propagation,* vol. 2, pp. 736-747, 2015.

[20] G. Efstathopoulos and A. Manikas, "Extended array manifolds: Functions of array manifolds", IEEE Transactions on Signal Processing, vol. *59*(7), pp. 3272-3287, 2011.

[21] D. M. Kitavi, H. Tan, and K. T. Wong, "A regular tetrahedral array whose constituent sensors fail randomly—A lower bound for direction-of-arrival estimation", *In 2016 Loughborough Antennas & Propagation Conference (LAPC)* IEEE pp. 1-5, 2106.

[22] D. M. Kitavi, T. C. Lin, and K. T. Wong, "A tetrahedral array of isotropic sensors, each suffering a random complex gain—the resulting hybrid Cramér-Rao bound for direction finding*", In 2016 IEEE National Aerospace and Electronics Conference (NAECON) and Ohio Innovation Summit (OIS) IEEE,* pp. 412-415), 2016.

[23] S. Bindu, G. Singh, and I. Sarkar, "Study of DOA Estimation Using Music Algorithm," *International Journal of Scientific & Engineering Research,* vol. 6, pp. 2229-5518, July 2015.

[24] S. N. Bhuiya, F. Islam, and M. A. Matin, "Analysis of Direction of arrival techniques using uniform linear array," *International Journal of Computer Theory and Engineering,* vol. 4, pp. 931, 2012.

[25] X. Yuan, "Cramer-Rao bound of the direction-of-arrival estimation using a spatially spread electromagnetic vector-sensor," *In statistical signal processing workshop,* pp. 1-4, June 2011.

[26] P. Gupta and V. Verma, "Optimization of MUSIC and Improved MUSIC Algorithm to Estimate Direction of Arrival" International *Journal of Image, Graphics and Signal Processing*, pp. *8*(12), vol. 30, 2016.

[27] J. Serra, L. Blanco, and M. Najar, "Cramer-Rao bound for time-delay estimation in the frequency domain", *In 2009 17th European signal processing conference,* pp. 1037-1041, 2009.

[28] G. P. Gera and B. Mulgrew, "Antenna array cram´er-rao bound design by element relocation", *In 2007 17th European signal processing conference*, pp. 1141-1145, 2009.

[29] X. Yuan, "Cramér-Rao bounds of direction of arrival and distance estimation of a near field incident source for an acoustic vector sensor: polynomial-phase source", *IET Radar, sonar, and navigation*, vol. 6, pp. 638-648, 2012.

[30] P. Stoica, A. Nehorai, "Performance study of conditional and unconditional direction of arrival estimation," *IEEE Trans. on Acoustics Speech and Signal Processing*, vol. 38, no. 10, pp. 1783-1795, October 1990.

[31] H. Abeida and J. P. Delmas, "Gaussian Cramer-Rao bound for direction estimation of non-circular signals in unknown noise fields", *IEEE Transactions on Signal processing*, vol. 53(12), pp. 4610-8, 2005.

[32] D. M. Kitavi, K. T. Wong, and C. C. Hung, "An L-Shaped Array with Nonorthogonal Axes-Its Cram´er Rao Bound for Direction Finding," *IEEE Transactions on Aerospace and Electronic Systems*, vol. 54, pp. 486492, 2017.

[33] M. A. Yaqoob, A. Mannesson, B. Bernhardsson, N. R. Butt, and F. Tufvesson, "On the performance of random antenna arrays for direction of arrival estimation," *In Communications Workshops (ICC), 2014 IEEE International Conference,* pp. 193-199, June 2014.

[34] J. Shim, H. Park, G. Suk, C. B. Chae, and D. K. Kim, "Cram´er-Rao Lower Bound for DoA Estimation with RF Lens-Embedded Antenna Array," *arXiv preprint arXiv*, pp. 1612.04130, 2016.

[35] Y. B. Nechaev and I. W. Peshkov, "Measuring of False Peaks Occurring via Planar Antenna Arrays DOA Estimation," *International Journal of Advances in Telecommunications, Electrotechnics, Signals and Systems,* vol. 22, pp. 4551, May 2017.

[36] Y. Nuchae and I. Peshkov, "Accuracy Researching of Direction-of-Arrival Estimation Via Music for Circular, Octagonal, Hexagonal and Rectangular Antenna Arrays", *International Journal of Research in Engineering and Science (IJRES)*, vol. 4, pp. 08-15, 2016.

[37] F. Römer and M. Haardt, “Deterministic Cramér-Rao bounds for strict sense non-circular sources,” *In Proc. ITG/IEEE Workshop on Smart Antennas (WSA),* February, 2007.

[38] A. M. Montaser, K. R. Mahmoud, A. B. Abdel-Rahman and H. A. Elmikati, “Circular, Hexagonal and Octagonal Array Geometries for Smart Antenna System Using Hybrid CFO-HC Algorithm,” *Journal of Engineering Sciences, Assiut University*, vol. 40, no. 6, pp. 1715-1732, November 2012.

[39] K. R. Mahmoud, M. El-Adawy, and S. M. M. Ibrahem, “A comparison between circular and hexagonal array geometries for smart antenna systems using particle swarm optimization algorithm”, *Progress in Electromagnetics Research,* pp. 75-90, 2007.

[40] S. Kiani and A. M. Pezeshk, “A Comparative Study of Several Array Geometries for 2D DOA Estimation”, *Procedia computer science,* vol. 58, pp. 18-25, 2015.

[41] S. Sharma, G. Singh, and I. Sarkar, “Study of DOA Estimation Using Music Algorithm”, *International Journal of Scientific & Engineering Research,* vol. 6, 2015.

[42] M. Devendra and K. Manjunathachari, “DOA estimation of system using MUSIC method,” *In Signal Processing and Communication Engineering Systems International Conference,* pp. 309-313, January 2015.

[43] U. Baysal and R. L. Moses, “Optimal Array Geometries for Wideband DOA Estimation OHIO*”, state univ columbus dept of electrical engineering,* 2001.

[44] S. Cho, K. J. You, and H. C. Shin, “A new direction-of-arrival estimation method using automotive radar sensor arrays”, International Journal of Distributed Sensor Networks, vol. *13*(6), pp. 1550147717713628, 2017.

[45] H. Xiong, “Antenna array geometries and algorithms for direction of arrival estimation,” *Doctoral dissertation, University of Nottingham,* 2013.

[46] C. M. Tan, M. A. Beach, and A.R. Nix, “Problems with direction finding using linear array with element spacing more than half wavelength”, *1st Annual COST 273 Workshop, Espoo, Finland,* 2002.

[47] S. Kiani and A. M. Pezeshk, “A comparative study of several array geometries for 2D DOA estimation,” *Procedia Computer Science*, vol. 58, pp. 18-25, 2015.

[48] X. Lan, L. Wan, G. Han, and J. J. Rodrigues, “A novel DOA estimation algorithm using array rotation technique,” *Future Internet,* vol. 6, pp. 155-170, 2014.

[49] G. Peter, X. Angeliki and M. Christoph, “Multiple and single snapshots compressive beamforming”, The *Journal of Acoustical Society of America,* pp. 1 - 12, August 2015.

[50] R. Joshi and D. Ashwinikumar, “Direction of arrival estimation using MUSIC algorithm,” International *Journal of Research in Engineering and Technology*, vol. 3, pp. 633-636, 2014.

[51] J. G. Hong, W. H. Ahn, and B. S. Seo, “Compensation of Mutual Coupling in an Antenna Array for Direction of Arrival Estimation”, pp. 599-603, 2013.

[52] M. Sitakanta and M. Mainak, “A Novel 2 directional blind direction of arrival estimation algorithm for smart antenna”, *International Journal of Engineering Research and Technology*, vol. 06, pp. 133 - 140, June 2015.

[53] F. Römer and M. Haardt, “Deterministic Cramér-Rao bounds for strict sense non-circular sources,” In *Proc. ITG/IEEE Workshop on Smart Antennas (WSA)*, 2007, February.

[54] D. M. Kitavi, K. T. Wong, M. Zou, and K. Agrawal, “Lower bound of the estimation error of an emitter's direction-of-arrival/polarisation, for a collocated triad of orthogonal dipoles/loops that fail randomly,” *The institution of engineering and technology,* vol. 11, pp. 961-970, 2017.

APPENDICES

Appendix I: Note on publication

Paper Published

G. W. Ndiritu, D. M. Kitavi, and C. G. Ngari, “Cramér-rao bound of direction finding using uniform hexagonal array”, *Journal of advances in Mathematics and computer science*, vol. 32(6), pp. 1-14, 2019.